Nonlinear finite element analysis of double skin composite columns subjected to axial loading

Süleyman İpek[1] · Esra Mete Güneyisi[2]

Abstract

The study aimed to simulate the behavior of the concrete-filled double skin steel tubular (CFDST) composite columns having a circular hollow section using the finite element method (FEM). To indicate the accuracy and the reliability of the model, the proposed FEM model was verified by the experimental test results available in the literature. Moreover, the code-based formulas (ACI, AISC, and Eurocode 4) and some empirical models suggested by the previous researchers for predicting the axial capacity of CFDST columns were used in this study to compare their results with the proposed FEM model. Furthermore, to visualize the effectiveness of sectional properties and infilled concrete compressive strength on the ultimate axial strength of double skin composite columns, a parametric study was conducted. For this, 72 test specimens were modeled considering two outer and inner steel tube diameters, three outer and inner steel tube thicknesses, and two different concrete cylinder strengths. All results were statistically evaluated. It was observed that the proposed FEM model had a good prediction performance. As well, the FEM model results indicated that the sectional properties, in particular, the diameter of the outer steel tube and concrete compressive strength, had remarkable effects on the load-carrying capacity of CFDST columns.

Keywords Axial loading · CFDST columns · Circular hollow section · FEM · Modeling

1 Introduction

The composite columns are one of the most important structural members that are the combination of structural concrete and steel. The composite columns have various shapes as shown in Fig. 1. Reinforced concrete columns are the composite column in which the reinforcing (steel) bars are surrounded by the concrete to resist against loads by acting together as shown in Fig. 1a. Indeed, concrete-encased steel columns are a special kind of composite column in which H-shaped steel is encompassed by concrete or reinforced concrete to improve the load-carrying capacity and earthquake resistance characteristic of columns as illustrated in Fig. 1b. Moreover, concrete-filled steel tubular (CFST) columns are a special type of composite column that consists of a steel tube filled with concrete as shown in Fig. 1c [1].

CFST columns have large strength and good deformability characteristics which makes it precious structural members [2]. Construction of these types of columns is quicker than that of traditional one, since the steel tube is also playing formwork role during the construction [3]. The CFST columns may be in various cross-sectional patterns. The common cross-sectional patterns of the CFST columns are given in Fig. 2 [4]. Figure 2a illustrates the common patterns of the CFST columns where B and D are the outer dimensions and t is the thickness of the steel tube. The patterns presented in Fig. 2b may be used for architectural purposes to achieve esthetic view in the structures. Offshore and marine structures, bridge pipers, and multi-floor structures are some of the utilization areas of CFST columns. The large lateral stiffness and strength, as well as the large load-carrying capacity that is obtained by a steel tube and concrete interaction, are sufficiently procured in the CFST columns. Besides, the steel tube secures the concrete that results in procrastination of the local buckling of the steel tube and also, the strength increment is provided to concrete by steel tube confinement effect [5]. There have been many studies carried out to experimentally and analytically investigate the behavior, characteristics, and application of CFST

✉ Süleyman İpek
   sipek@bingol.edu.tr

1 Department of Architecture, Bingöl University,
   12000 Bingöl, Turkey

2 Department of Civil Engineering, Gaziantep University,
   27310 Gaziantep, Turkey

Fig. 1 Typical sections of composite columns: **a** reinforced concrete column, **b** concrete-encased steel column, and **c** concrete-filled steel column [1]
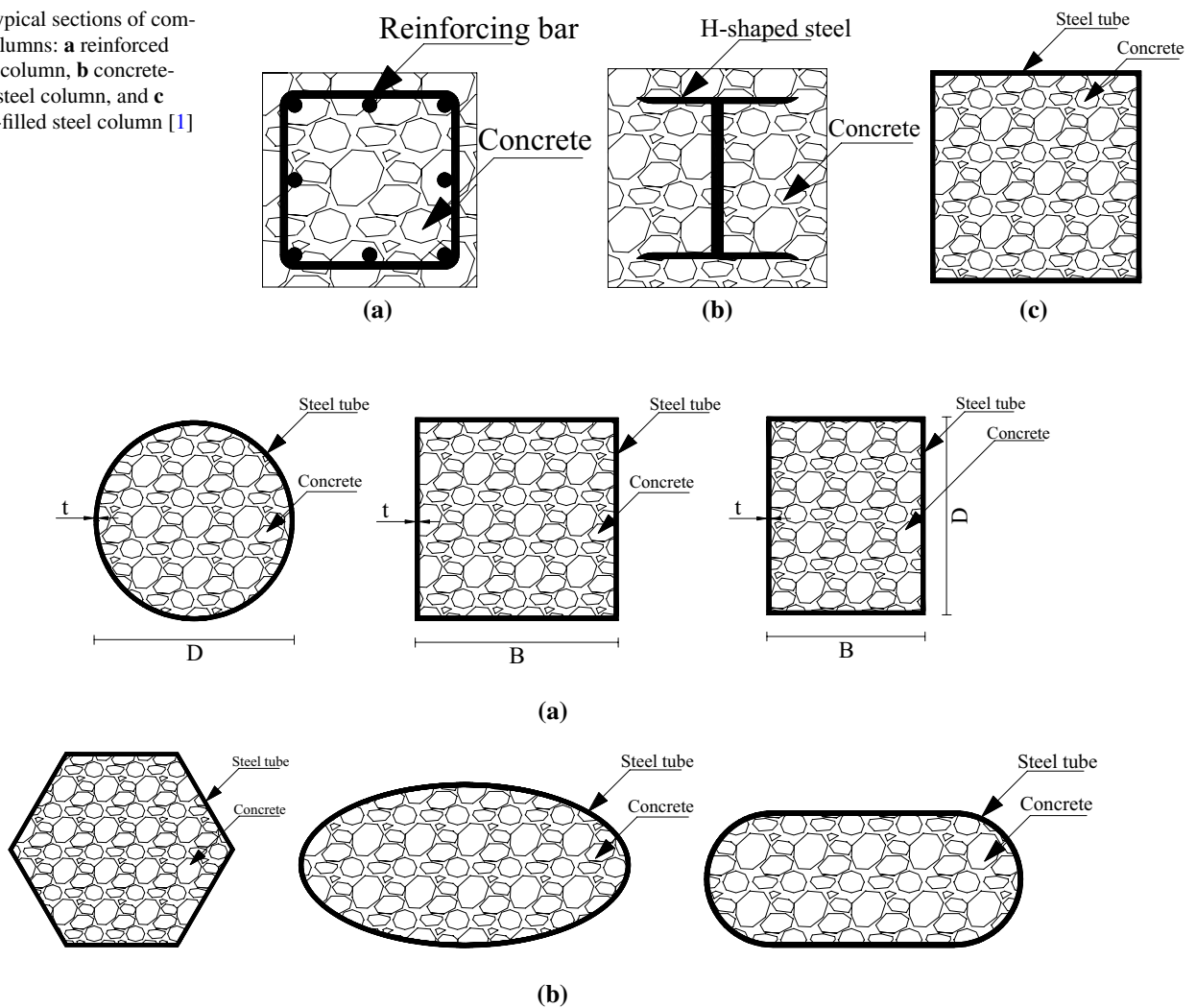
Fig. 2 Cross-sectional patterns of CFST columns: **a** common and **b** special configurations [4]

members [6–25]. For example, in 1967, Furlong [6] tested round and squared short columns under axial load and bending moments. Then, in 1971, Chen and Chen [7] theoretically analyzed the circular and square CFST beam-columns under symmetric and unsymmetric loading conditions. In 1990s, Lin [8], Luksha and Nesterovich [9], Prion and Boehme [10], Kato [11], and Morino et al. [12] experimentally investigated the short and long circular and square CFST columns under different loading conditions. In 2000, O'Shea and Bridge [13] developed several design methods to predict the strength of concrete-filled steel short columns under different types of loading. Elchalakani et al. [14] investigated the concrete-filled circular steel columns under pure bending and Elremaily and Azizinamini [15] studied the strength and behavior of concrete-filled steel columns with circular section. While Han et al. [16] examined the performance of such types of columns under cyclic loadings, Fujimoto et al. [17] and Wheeler and Bridge [18] examined the behavior of

such columns under the eccentrical and flexural loading conditions, respectively. Goode and Lam [19] compared the test results of about 1800 samples with the design code. Zhang et al. [20] investigated the circular CFST columns under seismic actions; whereas, Roeder et al. [21] investigated the strength and stiffness of such column types. Apart from the aforementioned researchers, Ho et al. [22] examined the behavior of the tie connected concrete-filled steel columns under the uniaxial loading. Lu et al. [23], Nour and Güneyisi [24], and Güneyisi et al. [25] proposed the empirical models to estimate the ultimate axial strength of CFST columns using different methods.

Concrete-filled double skin steel tubular (CFDST) members could be acknowledged as a new generation of conventional CFST members differing in some points. The general phenomenon for these members is the steel–concrete–steel formation. Namely, they are formed by two eccentrically built steel tubes and a concrete annulus between the tubes.

However, in some applications, the steel–concrete–steel–concrete phenomenon could be used. The general names for these phenomena are the hollow section and solid section, respectively. Figure 3 presents some types of CFDST member sections in detail. In the figures, D, D_o, D_i, B, B_o, and B_i, are the outer and inner dimensions of circular and square steel tubes, t_o and t_i are the thickness of outer and inner steel tubes, respectively. The circular hollow section (CHS) and the square hollow section (SHS) are illustrated in Fig. 3a, 3c, respectively. Figure 3b, d indicates the sections consisting of different shaped steel tube sections; as seen in Fig. 3b, the section comprises of outer circular and inner square steel tubes; whereas, in Fig. 3d, the section consists of outer square and inner circular tubes. All these sections are known as the hollow section [26].

In recent years, several experimental studies have been conducted on the behavior of the CFDST members [2, 26–32]. For example, Uenaka et al. [2] experimentally tested CFDST stub columns with CHS. They regarded the inner–outer diameter (D_i/D_o) ratio and diameter–thickness (D/t) ratio as testing parameters. They produced a totally of 12 stub columns specimen with changing the outer and inner steel tube thicknesses, the inner steel tube diameter, and the yield strength value of outer and inner steel tubes. They concluded that the failure mode of CFDST columns was local buckling occurring at both tubes that is due to accommodation to shear failure of the sandwiched concrete. Moreover, they inferred that the confinement effect that occurs on the concrete annulus significantly improves the strength of the CFST columns but in CFDST columns, the improvement, thanks to confinement effect, gradually decreased by increasing D_i/D_o. In addition, they observed that the plastic deformability of the CFDST specimen is almost similar to that of CFST. As a result, they claimed that the inner tube has no confinement effect because of complex biaxial compression. Essopjee and Dundu [26] manufactured 32 CFDST slender columns with CHS to measure their ultimate axial capacity under compressive loading. They altered the length and diameters of the specimens and the yield strength of the outer steel tube. According to their test results, it was

Fig. 3 Sections of CFDST columns: **a** circular outer and inner hollow section, **b** circular outer and square inner hollow section, **c** square outer and inner hollow section, and **d** square outer and circular inner hollow section [26]
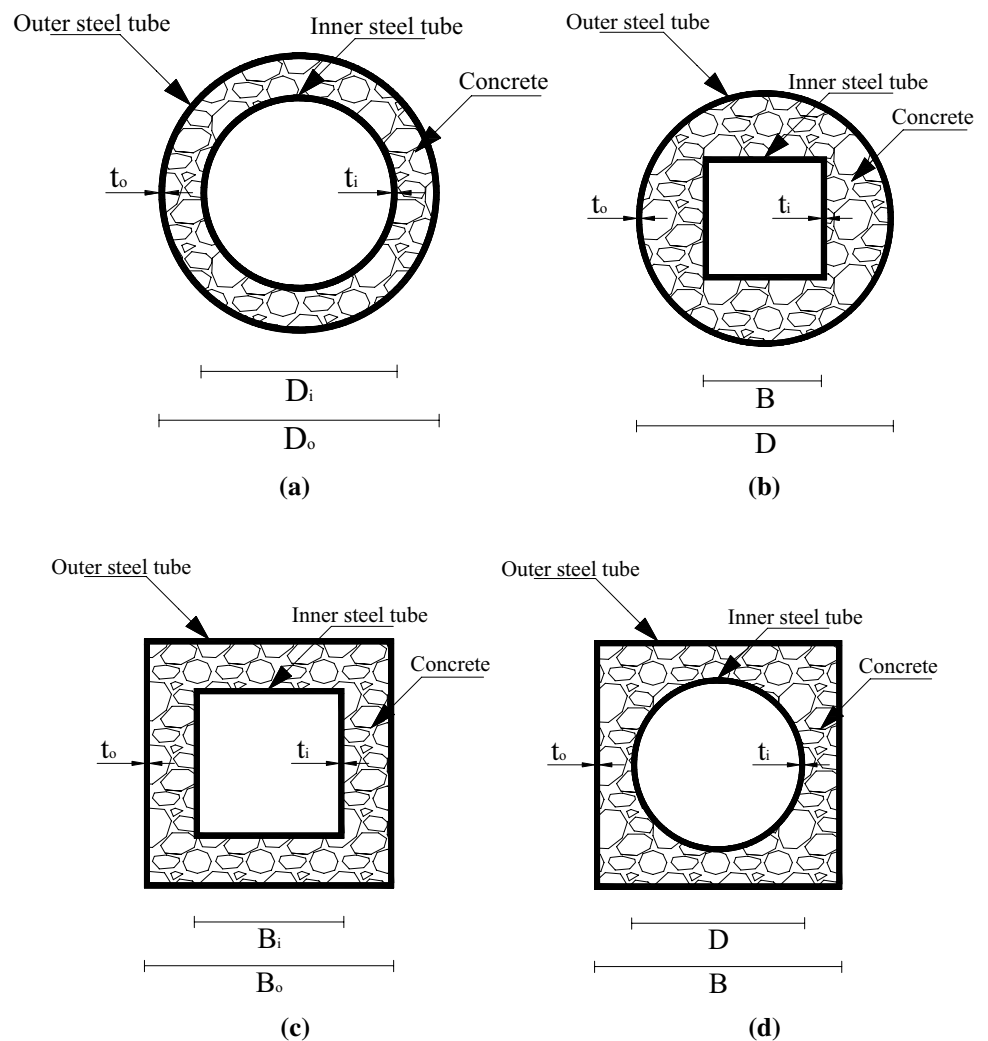
concluded that the CFDST columns having a length of 1 m failed due to the yield strength of the steel tubes; whereas, the columns having a length of more than 1 m failed owing to overall buckling that is the result of large slenderness. In addition, they verbalized that increasing the length of the columns specimens resulted in the reducing of the compressive capacity of the CFDST columns. Besides, they observed that the ultimate compressive strength of the specimens was increased by increasing the diameters. Zhao et al. [27] performed a series of compression tests on CFDST stub columns with CHS regarding six different section sizes for the outer tube and two different section sizes for the inner tube. They experimentally investigated the failure modes, strength, ductility, and energy absorption characteristics of CFDST stub columns with CHS. They disclosed two failure modes for the outer tube which was described as "elephant foot mode" and "diagonal shear mode"; while there was only one type of failure mode for the inner tube which was defined as "distorted diamond". Tao et al. [28] studied on CFDST stub columns and beam-columns. In this research, the sections of both inner and outer steel tubes were CHS. They considered the diameter–thickness and hollow section ratios for the stub columns and the slenderness ratio and the eccentricity of load for the beam-columns as main experimental parameters. Totally, 26 CFDST columns with CHS were tested and their ultimate axial strength, axial strain, and ductility index values, as well as the buckling modes, were determined in their study. They paid attention to "composite action" terms as a conclusion. They revealed that both column types, stub column and beam-column, have indicated relatively ductile behavior and the structural behavior of stub columns was enhanced thanks to the composite action between the steel tube and the concrete core. Han et al. [29] studied the long-term sustained loading and the ultimate strength test of the CFDST columns. For this purpose, 8 CFDST columns with CHS and 8 CFDST columns with SHS were manufactured. From each section, 5 column specimens were tested regarding only ultimate strength. It was specified that when the column specimens tested under long-term sustained load were compared with that tested under ultimate strength, lower ultimate axial capacity was observed. Wang et al. [30] investigated the effect of fiber-reinforced polymer on the ultimate axial capacity of the CFDST stub columns with CHS. They covered the CFDST stub columns with a different orientated fiber-reinforced polymer to increase the confinement effect. For this reason, they produced two CFDST stub columns with CHS excluding the fiber-reinforced polymers. It was observed that decreasing the concrete annulus cross section resulted in lower ultimate axial strength capacity of the CFDST stub columns with CHS. Lu et al. [31] examined the fire effect on the CFDST columns. In total, 18 CFDST columns with circular and square cross sections were manufactured during the study. Two of the total specimens were reference specimens that were not exposed to fire. One specimen was a reference for circular series, whereas the other was for square series. Wang et al. [32] conducted an experimental study on CFDST stub columns with CHS to investigate their strength and behavior. In total, 14 column specimens were manufactured with various concrete class and inner tube diameter and thickness. The gap between the outer and inner steel tube was filled with three different concrete cylinder strengths of 40, 80, and 120 MPa. The strength of CFDST stub columns with CHS was measured by applying uniform axial loading; whereas the behavior was studied with respect to failure mode and load–axial strain relationship. It was reported that the collapsing shape of the columns was a ductile failure. Moreover, in the literature, there are some numerical works on the CFDST members [33–35] in which the diameter–thickness ratio of outer and inner steel tubes, steel tube yield strength, hollow ratio, and the length of column specimen were mainly studied.

However, apart from the above researches, the study presented herein includes the nonlinear analysis of the CFDST columns with CHS under axially loading conditions, as shown in Fig. 4. Accordingly, the finite element method (FEM) was used to model and analyze the CFDST columns, and the experimental test results available in the literature were utilized to verify the reliability and accuracy of the model. After the verification of the FEM model, 72 CFDST column specimens were modeled with two outer and inner steel tubes diameters, three outer and inner steel tubes thickness, and two different concrete cylinder strengths to visualize the influences of sectional characteristics and infilled concrete compressive strength on the ultimate axial strength of double skin composite columns. Thereafter, the formulas modified from the codes and the suggested empirical models by the previous researchers were used to predict the ultimate axial strength of these 72 modeled test specimens. Also, the results were statistically evaluated to indicate the prediction performance of the models and understand which the parameters of the CFDST columns were effective on the ultimate capacity.

2 Modeling by finite element method (FEM)

The finite element program named ABAQUS CAE 16 [36] was employed to simulate and analyze the nonlinear behavior of the CFDST columns with CHS under axially loading conditions. The material definition, especially the nonlinear behaviors, interaction and surface identifications, the element type, and mesh selection, and loading and boundary conditions are presented in detail in the following sections. Moreover, the flow chart that indicates the use of the finite element software step by step has been presented in Fig. 5.

Fig. 4 Specimen details and test configuration of CFDST columns with CHS
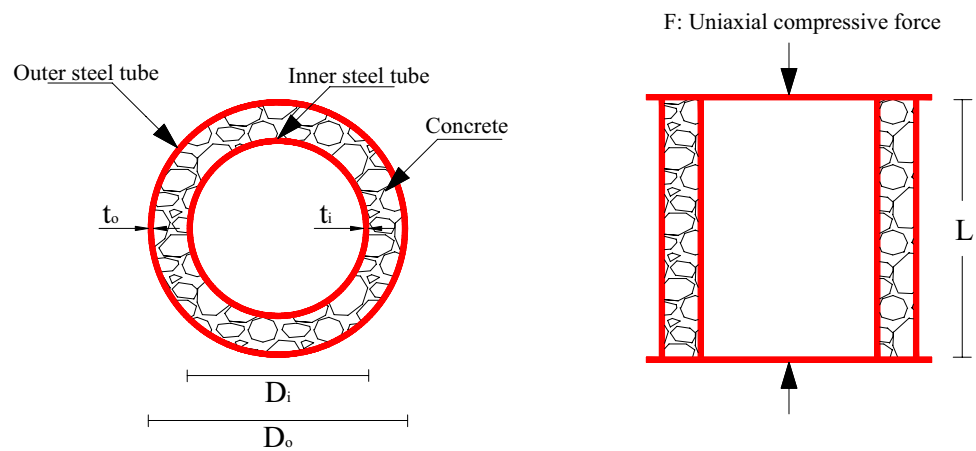
2.1 Material modeling

In this study, the CFDST columns with CHS consist of two steel tubes named outer and inner, two end plates placed at the top and bottom of columns, and the concrete annulus between the steel tubes. The material behaviors of steel and concrete are explained in the following sections.

2.1.1 Modeling of steel

In ABAQUS, bilinear elastic–plastic material behavior with isotropic hardening was considered for modeling of both end plates and steel tubes. According to the recommendation by Han and Huo [37], the stress–strain relationship consists of two regions as shown in Fig. 6. The elastic characteristics of the steel were specified in the first region, which starts from the origin and ends at the yield point. The elastic constants such as modulus of elasticity and Poisson's ratio were set in this region. The modulus of elasticity was used as 200×10^3 N/mm^2 and Poisson's ratio, ν_s, for all steel tubes was considered as 0.3.

The modulus of elasticity of the steel was used for the determination of modulus in a plastic region that was assumed to be equal to 1% of elastic modulus. First and second regions, namely elastic and plastic regions, could be easily achieved using the following equations [34]:

$$\sigma_i = E_s \varepsilon_s \quad \text{for } \varepsilon_s \leq \varepsilon_{sy}(\text{elastic region}), \tag{1}$$

$$\sigma_i = f_{sy} + E_p(\varepsilon_s - \varepsilon_{sy}) \quad \text{for} \varepsilon_s > \varepsilon_{sy}(\text{plastic region}), \tag{2}$$

where σ_i is the desired steel strength, E_s is the modulus of elasticity of steel, ε_s is the strain of steel, f_{sy} is the yield strength of steel, ε_{sy} is the strain of steel at yield point (calculated by f_{sy}/E_s).

As a result, the steel behavior was defined in ABAQUS as elastic till its yield strain and plastic between yield and final strain that was assumed to be 3% in this study.

2.1.2 Modeling of concrete

The confinement effect provided by the surrounding steel can be considered in the case of a lower diameter–thickness ratio (D_o/t_o) of the outer steel tube. Otherwise, the confinement effect on concrete procured by steel would be insufficient. For this reason, the strength improvement in concrete ensured by confinement effect could be considered in the case of D_o/t_o is less than or equal to 150. In the modeling of concrete in ABAQUS, two different concrete stress–strain relationships, confined and unconfined, could be identified as indicated in Fig. 7 [38].

In Fig. 7, f_c' and f_{cc} are the unconfined compressive strength of cylinder concrete, which is equal to 80% of compressive strength of cube concrete, and confined compressive strength, respectively. The corresponding strains of unconfined and confined concretes are demonstrated by ε_c and ε_{cc}, respectively. The compressive strength of cylinder concrete can be obtained by experimental test and the unconfined concrete strain, ε_c, can be considered as 0.003 regarding ACI [39] suggestion. However, the following formulas proposed by Mander et al. [40] could be used in the calculation of the confined concrete parameters, strength and corresponding strain:

$$f_{cc} = f_c' + k_1 f_1, \tag{3}$$

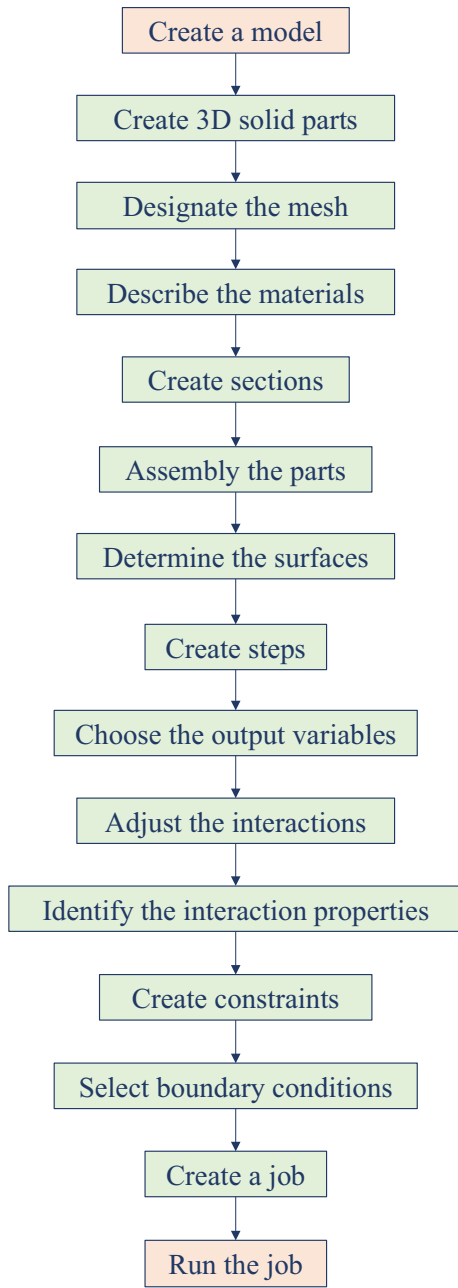$$\varepsilon_{cc} = \varepsilon_c \left(1 + k_2 \frac{f_1}{f_c'}\right), \tag{4}$$

Fig. 5 Flow chart indicating the use of finite element software

Fig. 6 Stress–strain curve for steel end plates and tubes [37]
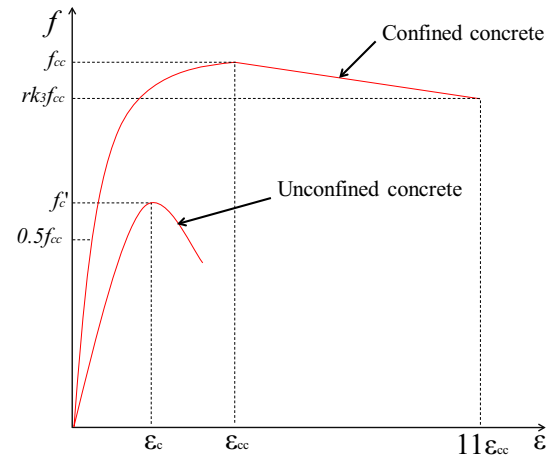
Fig. 7 Stress–strain curves for confined and unconfined concrete [38]

$$f_1 = f_{syo}\left[0.006421 - 0.0000357\left(\frac{D_o}{t_o}\right)\right], \tag{6}$$

where D_o, t_o, and f_{syo} are the diameter, thickness, and yield strength of the outer steel tube, respectively.

As clearly be seen from Fig. 7, the confined concrete stress–strain curve contains three zones. The elastic region, which begins from the origin and ends at the proportional limit stress, is the first zone of the curve; while the nonlinear region, which falls between the proportional limit and confined concrete stresses, is the second zone of the stress–strain curve of the confined concrete. In this study, the proportional limit stress was taken as $0.5f_{cc}$ according to proposal by Hu et al. [38] and the corresponding strain was calculated by dividing the proportional limit stress to

where k_1 and k_2 are the constants recommended by Richart et al. [41] to be taken as 4.1 and 20.4, respectively, f_1 is the lateral confining pressure provided by the steel tube (calculated with Eqs. 5 and 6 recommended by Hu et al. [38]).

In the case of $21.7 \le D_o/t_o \le 47$,

$$f_1 = f_{syo}\left[0.043646 - 0.000832\left(\frac{D_o}{t_o}\right)\right]. \tag{5}$$
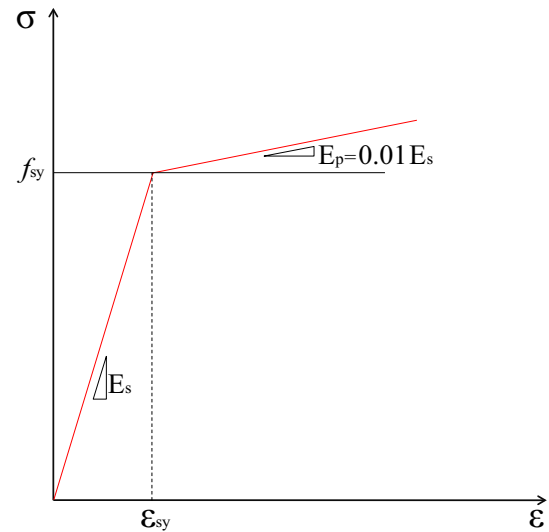
In the case of $47 < D_o/t_o \le 150$,

confined concrete's modulus of elasticity, E_{cc}. The empirical equation given as follows and suggested by ACI [39] was used to determine the acceptably elastic modulus for the confined concrete (Eq. 7). In addition to that, the Poisson's ratio for conventional concrete, ν_c, ranges between 0.15 and 0.22 and it was presumed to be 0.19 for confined concrete in this numerical analysis.

$$E_{cc} = 4700\sqrt{f_{cc}}. \tag{7}$$

The nonlinear region of the stress–strain curve of the confined concrete could be determined by the following expression that was recommended by Saenz [42]:

$$f' = \frac{E_{cc}\varepsilon}{1 + \left(R + R_E - 2\right)\left(\frac{\varepsilon}{\varepsilon_{cc}}\right) - (2R - 1)\left(\frac{\varepsilon}{\varepsilon_{cc}}\right)^2 + R\left(\frac{\varepsilon}{\varepsilon_{cc}}\right)^3}, \tag{8}$$

where ε is the strain in the nonlinear region of concrete, R and R_E are the coefficients to be calculated by the following expressions:

$$R = \frac{R_E\left(R_\sigma - 1\right)}{\left(R_\varepsilon - 1\right)^2} - \frac{1}{R_\varepsilon}, \tag{8a}$$

$$R_E = \frac{E_{cc}\varepsilon_{cc}}{f_{cc}}, \tag{8b}$$

where R_σ and R_ε are set to be equivalent to 4 according to the suggestion by Hu and Schnobrich [43].

In this situation, in the formula proposed by Saenz [42], only the strain, ε, value is unknown to calculate the stress. The stress values for the nonlinear region could be easily computed by postulating the strain values which must be between the proportional strain and the confined strain.

The third zone of the stress–strain curve of confined concrete could be named as a descending region which starts from the confined concrete strength and decline throughout the terminated stress value of the curve that can be computed as $rk_3 f_{cc}$. The strain value at the terminated stress was formulized to be $11\varepsilon_{cc}$. It was recommended by Hu et al. [38] that the coefficient, k_3, used in the calculation of the last point of the descending region can be computed by the following expressions:

In the case of $21.7 \le D_o/t_o \le 47$,

$$k_3 = 1. \tag{9}$$

In the case of $47 < D_o/t_o \le 150$,

$$k_3 = 0.0000339\left(\frac{D_o}{t_o}\right)^2 - 0.0100085\left(\frac{D_o}{t_o}\right) + 1.3491. \tag{10}$$

The other coefficient in the final stress calculation, r, was proposed to be taken as 1.0 for the concrete having 30 MPa cube strength, f_{cu}, and 0.5 for the concrete having the cube strength, f_{cu}, more than 100 MPa. This recommendation by Ellobody and Young [44, 45] depends on the experimental study carried out by Giakoumelis and Lam [46]. The linear interpolation could be carried out to determine the concrete having the cube strength, f_{cu}, between 30 and 100 MPa.

The confined concrete was identified as a material consisting of the elastic and plastic regions. In the ABAQUS, the Drucker–Prager yield criterion model was used to compute the plastic characteristics of the confined concrete which was the second and third zones of the stress–strain curve of the confined concrete. The shear criterion in the Drucker–Prager model was chosen as linear and flow potential eccentricity was selected as the default value of 0.1. Furthermore, the other three parameters in the Drucker–Prager model were the material angle of friction, the flow stress ratio of the material, and the dilation angle. The material angle of friction and the flow stress ratio in triaxial tension to that in compression were computed as 20° and 0.8 regarding recommendation by Hu et al. [38]; whereas, the dilation angle was selected according to Damaraju [47] as 30°. In addition to Drucker–Prager parameters, Drucker–Prager Hardening was chosen as a suboption to accurately define the yield region of the confined concrete. It is worthy to note that Drucker Hardening suboption parameters such as the yield stress and absolute plastic strain values, which are dependent on the concrete strength and confinement effect, were individually determined using Eqs. (3)–(10) for the confined concrete of each composite column.

2.2 Interaction and surface identifications

In the modeling of each specimen, endplates, which were placed at the top and bottom of columns, were used to attain equal contractions. In this way, each specimen consisted of five components such as outer and inner steel tubes, the concrete annulus between the tubes, and the top and bottom endplates as indicated in Fig. 8. The surfaces of the components were used to identify the interactions. The surface-to-surface contact and Tie constraint available in ABAQUS CAE [36] were employed to govern the bond between the specimen components. Using these methods, the surfaces should be first identified according to their characterizations, namely it should be decided which surface will penetrate to others. For this condition, in ABAQUS CAE [36], the surfaces can be defined as master or slave. In this study, the steel tube surfaces were selected as master surfaces during the interaction with concrete; whereas, they were designated as slave surfaces when interacted with endplates. The surfaces of endplates were treated as master surface, while the surfaces of the concrete annulus were chosen as slave surface in all interactions
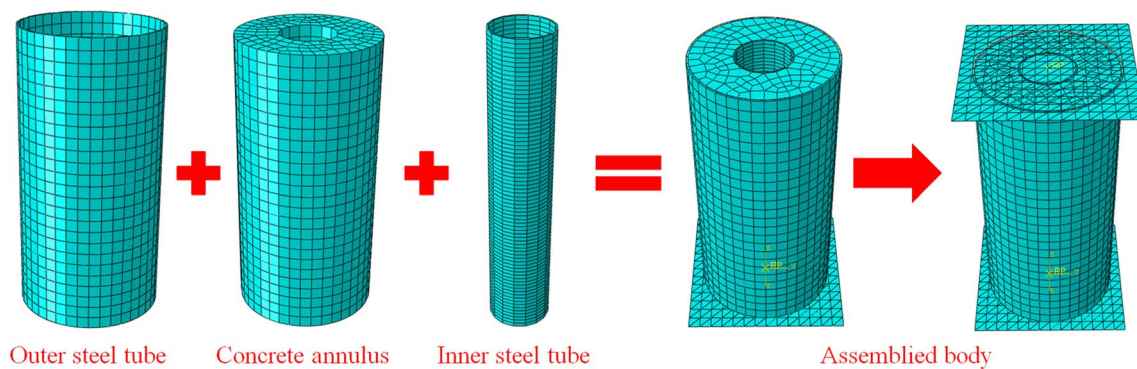
Fig. 8 The typical meshing of CFDST columns with CHS

with other components. Normal and Tangential behaviors were computed for the surface-to-surface contact properties. The pressure-overclosure model with hard contact feature was used for normal behavior; whereas, the penalty friction model with a friction coefficient of 0.3 and directionality of isotropic was applied for Tangential behavior. The surface-to-surface contact was designated to define the interactions between the surfaces of the steel tubes and the concrete annulus and also between the surfaces of the end plates and the concrete annulus. Tie constraint, however, was used to identify only the interactions between the steel tubes and endplates surfaces excluding the interaction between the inner steel tube and top endplate. For this interaction, the surface-to-surface contact was chosen.

2.3 Finite element type and mesh selection

The components in this study were modeled with respect to the solid and shell shapes. The solid-shaped components were sketched using extrusion type; while the shell-shaped elements were drawn using planar type. The outer and inner steel tubes and the concrete annulus between tubes were deformable solid shaped, whereby the endplates were discrete rigid shell shaped. R3D3 element type with geometric order of linear was used for the endplates; while the C3D8 element type with reduced integration and geometric order of linear was used for the outer and inner steel tubes and the concrete annulus. The element shape for R3D3 and C3D8 was triangle and hexahedron, respectively. The approximate global size of the mesh was 25 for the endplates. However, to achieve good meshing, the approximate global size of the mesh was 24 for outer steel tube and concrete annulus and 8 for the inner. The representative meshing of each component is illustrated in Fig. 8. The aforementioned finite element meshing was determined by performing a mesh convergence studies to specify the optimal meshing, which yields a relative accurate solution having low computational time.

2.4 Boundary and loading conditions

There was a reference (RF) point in the top and bottom end plates to specify the center of the plates and create a rigid body constraint. The boundary and loading were applied to the specimens from these RF points. Encastre type boundary condition in ABAQUS CAE [36] was used at the bottom end plates to obtain fixed support against all degrees of freedom. However, the top plate on which the load was applied was unrestrained in the loading direction. The nodes remained in the specimen were free to displace or rotate in any direction. The static uniform loading by designating a displacement on the RF point of top endplate was applied to each specimen.

3 Modified and proposed empirical models

The ultimate axial strength of the concrete-filled single skin steel tubular columns can be easily calculated by the empirical methods presented in the codes. However, in the literature, for predicting the strength of the concrete-filled double skin steel tubular composite columns, the modified version of the formulas given in ACI [39], Eurocode 4 [48], and AISC [49] was used [26, 27, 32–35, 48]. In this study, the modified formulas were utilized as given below. In addition, in the literature, there are some proposed empirical models which were developed or derived by the researchers such as Uenaka et al. [2], Han et al. [50], Yu et al. [51], and Hassanein et al. [52]. This section also includes the explicit presentation of these proposed empirical models.

3.1 Formula modified from ACI [39]

ACI code [39] proffers an equation by which the ultimate axial strength of single skin composite columns containing a reinforcing bar can be determined. However, the concrete confinement effect is disregarded in the formula suggested by the ACI code [39]. The equation modified from ACI code

[39] to determine the ultimate axial strength of the CFDST stub column involving the contribution of the inner steel tube is expressed as follows [39]:

$$\left(P_u\right)_{ACI} = f_{syo}A_{so} + 0.85f_c'A_c + f_{syi}A_{si}, \tag{11}$$

where A_{so}, A_c, and A_{si} are the cross-sectional areas of outer steel tube, concrete annulus, and inner steel tube, respectively, and f_{syi} is the yield strength of the inner steel tube.

3.2 Formula modified from Eurocode 4 [48]

The equation suggested by Eurocode 4 (EC4) [48] for the calculation of the ultimate axial strength of the CFST columns includes the outer steel tube, reinforcing bars and concrete as well as confinement effect. EC4 [48] approach has two different equations according to relative slenderness criteria. The approach in EC4 [48] uses a reduction factor, η_a, and an enhancement factor, η_c, for the contribution of the steel to the cross-section resistance and for the concrete contribution, respectively, regarding the confinement effect of concrete. In these formulations, firstly, the reinforcement part was considered as a second steel skin. For this reason, the strength provided by this section was multiplied with η_a, the factor related to the confinement of concrete as recommended by Pagoulatou et al. [34]. Then, the terminological conversion was carried out. Finally, the following expressions were obtained for both conditions:

In the case of $\bar{\lambda} > 0.5$,

$$\left(P_u\right)_{EC4} = f_{syo}A_{so} + f_c'A_c + f_{syi}A_{si}. \tag{12}$$

In the case of $\bar{\lambda} \leq 0.5$,

$$\left(P_u\right)_{EC4} = \eta_a f_{syo}A_{so} + f_c'A_c\left[1 + \eta_c\left(\frac{t_o}{D_o}\right)\left(\frac{f_{syo}}{f_c'}\right)\right] + \eta_a f_{syi}A_{si}, \tag{13}$$

where η_a and η_c are the reduction factor for the contribution of the steel to the cross-section resistance and the enhancement factor for the concrete contribution, respectively. They are to be calculated as follows:

$$\eta_a = 0.25\left(3 + 2\bar{\lambda}\right)(\text{but} \leq 1.0), \tag{13a}$$

$$\eta_c = 4.9 - 18.5\bar{\lambda} + 17\bar{\lambda}^2(\text{but} \geq 0), \tag{13b}$$

where $\bar{\lambda}$ is the relative slenderness and to be determined by the following expression:

$$\bar{\lambda} = \sqrt{P_{pl,Rd,(6.30)}\big/P_{cr}}, \tag{13c}$$

where $P_{pl,Rd,(6.30)}$) is the characteristic value of the plastic resistance given in EC4 [48] as 6.30th equation and this

expression applies for concrete-encased and partially concrete-encased steel sections, to be determined by the following expression:

$$P_{pl,Rd,(6.30)} = f_{syo}A_{so} + 0.85f_c'A_c + f_{syi}A_{si}. \tag{13d}$$

P_{cr} is the elastic critical normal force for relevant buckling mode and to be determined by the following expression:

$$P_{cr} = \frac{\pi^2(EI)_{eff}}{\left(KL_u\right)^2}, \tag{13e}$$

where K is the effective length factor (for pin–pin connection can be taken as 1.0), L_u is the laterally unbraced length of the member, and EI_{eff} is the effective stiffness of composite section and to be calculated by the following expression:

$$EI_{eff} = E_{so}I_{so} + K_cE_{cm}I_c + E_{si}I_{si}, \tag{13f}$$

where E_{so}, E_{cm}, and E_{si} are the elastic modules of outer steel tube, concrete, and inner steel tube, I_{so}, I_c, and I_{si} are the inertias of outer steel tube, concrete, and inner steel tube sections, and K_c is a correction factor that should be taken as 0.6.

Herein, the modulus of elasticity of concrete could be calculated by the following equation provided by ACI-318 [39]:

$$E_{cm} = w_c^{1.5}0.043\sqrt{f_c'}, \tag{13g}$$

where w_c is the unit weight of the concrete (between 2300 and 2500 kg/m^3).

At the end of the calculation of the ultimate axial strength of the CFDST columns, the strength value should be multiplied with the reduction factor (χ) for the relevant buckling mode. The formula for the reduction factor according to Eurocode 3 [53] is as follows:

$$\chi = \frac{1}{\phi + \sqrt{\phi^2 - \bar{\lambda}^2}} \quad \text{but} \chi \leq 1.0, \tag{14}$$

in which;

$$\phi = 0.5\left[1 + \alpha\left(\bar{\lambda} - 0.2\right) + \bar{\lambda}^2\right], \tag{14a}$$

α is an imperfection factor depending on a buckling curve and can be taken from Table 6.1 in EC3 [53]. As Hassanein and Kharoob [35] mentioned in their study, the imperfection factor was taken according to the buckling curve (b) as 0.34.

3.3 Formula modified from AISC [49]

The equations by AISC [49] are suggested for the single skin composite columns involving reinforcing bars. AISC [49] also recommends two different expressions for the determination of the ultimate axial strength of encased composite columns that subjected to axial loading:

In the case of $P_e < 0.44P_o$

$$(P_u)_{AISC} = 0.877P_e, \tag{15}$$

in which;

$$P_e = \frac{\pi^2 (EI)_{eff}}{(KL)^2}. \tag{15a}$$

EI_{eff} can be calculated using Eq. 13f with a small alteration in the correction factor, K_c as given in the following expressions:

$$K_c = 0.6 + 2\left(\frac{A_{so}}{A_c + A_{so}}\right) \le 0.9. \tag{15b}$$

In the case of $P_e \ge 0.44P_o$,

$$(P_u)_{AISC} = P_o\left[0.658^{\left(\frac{P_o}{P_e}\right)}\right], \tag{16}$$

in which;

$$P_o = f_{syo}A_{so} + 0.95f'_c A_c + f_{syi}A_{si}. \tag{16a}$$

Herein, in the calculation of P_o and P_e, a steel tubular section instead of reinforcing bars was considered as a second skin. After these modifications, P_o and P_e can be expressed as above.

3.4 Empirical model proposed by Uenaka et al. [2]

Uenaka et al. [2] derived the equation determining the ultimate axial strength of the CFDST columns from the equation that was proposed by AIJ [54] for CFST stub columns. Uenaka et al. [2] elementally superposed strength of the tubes and the concrete infill between tubes. The following expression was first asserted to temporarily estimate the ultimate axial strength of CFDST:

$$P_u = f_{syo}A_{so} + f'_c A_c + f_{syi}A_{si}. \tag{17}$$

After the experimental tests, it was overemphasized that the confinement effect of the outer tube is more effective on the ultimate axial strength of the CFDST columns than that of the inner tube [2]. Regarding the experimental results, the estimated ultimate axial strength derived from AIJ [54] is modified to the following expression by Uenaka et al. [2]:

$$(P_u)_{UENAKA} = \left(2.86 - 2.59\left(\frac{D_i}{D_o}\right)\right)f_{yo}A_{so} + f'_c A_c$$
$$+ f_{yi}A_{si}\left(0.2 < D_i/D_o < 0.7\right), \tag{18}$$

where D_i is the diameter of the inner steel tube.

3.5 Empirical model proposed by Han et al. [50]

Han et al. [50] proposed an equation regarding the inner tube capacity and a capacity containing the outer steel tube and concrete annulus. The formula given by Han et al. [50] is as follows:

$$(P_u)_{HAN} = P_{osc,u} + P_{i,u}, \tag{19}$$

where $P_{i,u}$ and $P_{osc,u}$ are the capacity of the inner steel tube and the capacity of the outer steel tube and concrete annulus to be determined by Eqs. 19a and 19b, respectively.

$$P_{i,u} = f_{syi}A_{si}, \tag{19a}$$

$$P_{osc,u} = f_{osc}A_{soc}, \tag{19b}$$

where f_{osc} is the strength characteristic of outer steel tube and concrete annulus and to be determined by the following expression:

$$f_{osc} = C_1\chi^2 f_{syo} + C_2(1.14 + 1.02\xi)f_{ck}, \tag{19c}$$

where C_1 and C_2 are the strength coefficient of the outer steel tube and the concrete annulus, respectively, and to be determined by Eqs. 19d and 19e:

$$C_1 = \frac{\alpha'}{1 + \alpha'}, \tag{19d}$$

$$C_2 = \frac{1 + \alpha_n}{1 + \alpha'}, \tag{19e}$$

in which α' and α_n can be determined by Eqs. 19 and 19g:

$$\alpha' = \frac{A_{so}}{A_c}, \tag{19f}$$

$$\alpha_n = \frac{A_{so}}{A_{c,nominal}}. \tag{19g}$$

χ and ξ are the hollow section ratio and the nominal confinement factor, respectively, and to be determined by Eqs. 19h and 19i:

$$\chi = \frac{D_i}{D_o - 2t_o}, \tag{19h}$$

$$\xi = \frac{f_{syo}A_{so}}{f_{ck}A_{c,nominal}}, \tag{19i}$$

where f_{ck} and $A_{c,nominal}$ are the characteristic compressive strength and the nominal cross-sectional area of the concrete, respectively, and to be determined by Eqs. 19j and 19k:

$$f_{ck} = 0.67 f_{cu}, \tag{19j}$$

$$A_{c,nominal} = \frac{\pi (D_o - 2t_o)^2}{4}, \tag{19k}$$

where f_{cu} is the characteristic cube strength of concrete.

A_{soc} is the cross-sectional area of the outer steel tube and concrete annulus and to be determined by the following expression:

$$A_{soc} = A_{so} + A_c. \tag{19l}$$

3.6 Empirical model proposed by Yu et al. [51]

Yu et al. [51] proposed an equation confirming the experimental ultimate axial strength results. The formula was for the single skin solid and hollow section CFST columns and presented as follows:

$$P_u = \left(1 + 0.5\frac{\xi}{1+\xi}\Omega\right)(f_{sy}A_s + f_{ck}A_c), \tag{20}$$

where ξ and Ω are the confinement coefficient and the solid ratio, respectively, and to be determined by Eqs. 20a and 20b:

$$\xi = \frac{f_{syo}A_{so}}{f_{ck}A_c}, \tag{20a}$$

$$\Omega = \frac{A_c}{A_c + A_k}, \tag{20b}$$

where f_{sy} is the yield strength of steel tube, f_{ck} is the characteristic strength of concrete, and A_k is the cross-sectional area of the hollow part.

Herein, the formula proposed by Yu et al. [51] was modified to be applicable to the double skin CFST columns. As Hassanein and Kharoob [55] recommended, the modified formula includes the combination of circular hollow CFST column and inner steel tube as follows:

$$(P_u)_{YU} = \left(1 + 0.5\frac{\xi}{1+\xi}\Omega\right)(f_{syo}A_{so} + f_{ck}A_c) + P_{i,u}, \tag{21}$$

in which $P_{i,u}$ can be determined by Eq. 19a.

3.7 Empirical model proposed by Hassanein et al. [52]

Hassanein et al. [52] proposed a new design model for calculation of the ultimate axial strength of circular CFDST short columns based on Liang and Fragomeni's [56] design models for determining the ultimate axial strength of circular CFST short columns and Hassanein et al.'s [57] design models for calculating the ultimate axial strength of concrete-filled stainless steel tubular short columns and concrete-filled stainless steel–carbon steel tubular short columns. The new design model proposed by Hassanein et al. [56] is presented as follows:

$$(P_u)_{HASSANEIN} = \gamma_{so}f_{syo}A_{so} + (\gamma_c f_c' + 4.1f_1)A_c + \gamma_{si}f_{syi}A_{si}, \tag{22}$$

where γ_{so} and γ_{si} are the factor used to account for the influence of strain hardening on outer steel and inner steel tube, respectively, and to be determined by Eqs. 22a and 22b:

$$\gamma_{so} = 1.458\left(\frac{D_o}{t_o}\right)^{-0.1} \quad 0.9 \le \gamma_{so} \le 1.1, \tag{22a}$$

$$\gamma_{si} = 1.458\left(\frac{D_i}{t_i}\right)^{-0.1} \quad 0.9 \le \gamma_{si} \le 1.1, \tag{22b}$$

where t_i is the thickness of the inner steel tube.

γ_c is a strength reduction factor proposed by Liang [58] and to be determined by the following expression:

$$\gamma_c = 1.85D_c^{-0.135} \quad 0.85 \le \gamma_c \le 1.0, \tag{22c}$$

where D_c is the diameter of the concrete annulus and to be determined by the following expression:

$$D_c = D_o - 2t_o. \tag{22d}$$

f_1 is the lateral confining pressure and to be determined by the following expressions:

$$f_1 = \begin{cases} 0.7(v_o - v_s)\frac{2t_o}{D_o - 2t_o}f_{syo} & \text{for } \frac{D_o}{t_o} \le 47 \\ \left(0.006241 - 0.0000357\frac{D_o}{t_o}\right)f_{syo} & \text{for } 47 < \frac{D_o}{t_o} \le 150 \end{cases}, \tag{22e}$$

v_o is the Poisson's ratio of steel tube with concrete infill and to be determined by the following expression given by Tang et al. [59]:

$$\nu_o = 0.2312 + 0.3582\nu_o' - 0.1524\left(\frac{f_c'}{f_{syo}}\right)$$
$$+ 4.843\nu_o'\left(\frac{f_c'}{f_{syo}}\right) - 9.169\left(\frac{f_c'}{f_{syo}}\right)^2, \quad (22f)$$

in which

$$\nu_o' = 0.881 \times 10^{-6}\left(\frac{D_o}{t_o}\right)^3 - 2.58 \times 10^{-4}\left(\frac{D_o}{t_o}\right)^2$$
$$+ 1.953 \times 10^{-2}\left(\frac{D_o}{t_o}\right) + 0.4011, \quad (22f)$$

where ν_s is the Poisson's ratios of steel tube without concrete infill and at the maximum strength point, it is taken as 0.5.

4 Verification of the FEM model

The verification and calibration of the suggested model is a crucial issue to truthfully estimate the behavior of such columns. For this reason, the previously conducted experimental test results were considered in the verification and calibration of the proposed model. The test results of two samples, labeled as c16-1125 and c23-1125, from the study of Uenaka et al. [2] were used to affirm the FEM model. The CFDST column specimens from the study of Uenaka et al. [2] had the outer and inner steel tube yield strengths of 308 MPa for c16-1125-named sample and 286 MPa for c23-1125-named sample. In the preparation of both samples, the diameters of the outer steel tube were about 158–157 mm; whereas, it was 114–115 mm for the inner steel tube. The thickness of the outer and inner steel tubes was 1.5 mm for c16-1125-labeled sample and of the inner steel tube was 2.14 mm for c23-1125-labeled sample. In the manufacturing of both specimens, the concrete with the same compressive strength of 18.7 MPa was utilized and the length of the column specimens was 450 mm. For the verification of the FEM model, two CFDST column specimens from the study of Zhao et al. [27] were chosen. The specimens were labeled as C1C7 and C2C7 in this study. The outer steel tube yield strengths were 454 and 416 MPa, respectively; whereas, the yield strength of the inner steel tube for both specimens was 425 MPa. The diameters of the outer steel tube of these specimens were 114.5 and 114.6 mm, respectively, and the inner steel tube for both specimens had a diameter of 48.4 mm. The outer steel tube thickness of 2.8 mm was utilized in the manufacturing while the inner steel tube thickness of C1C7-named specimen was 5.9 mm and it was 4.7 mm for C2C7-named specimen. The concrete compressive strength of both specimens was about 63.4 MPa and their lengths were 400 mm.

In addition, four samples from the study of Tao et al. [28] and two samples from the study of Han et al. [26] were used to certify the developed FEM model. Tao et al. [28] and Han et al. [28] conducted the ultimate axial strength tests on two samples and the average of them was submitted. The samples with ID of cc4a, cc4b, cc7a, and cc7b were the selected CFDST column specimens from the study of Tao et al. [28]. The yield strength of the outer steel tube, the thicknesses of both steel tubes, and the compressive strength of the concrete part for all specimens taken from the study of Tao et al. [28] were same and they were 275.9 MPa, 3 mm, and 40 MPa, respectively. The outer and inner steel tube diameters for the cc4a- and cc4b-labeled samples were 180 and 48 mm, respectively; while the outer and inner steel tubes for the cc7a- and cc7b-labeled specimens had the diameters of 300 and 165 mm, respectively. The inner steel tubes of cc4a- and cc4b-named specimens had the yield strength of 342 MPa and that of cc7a and cc7b had the yield strength of 320.5 MPa. The lengths of cc4a- and cc4b-named specimens were 540 mm and it was 900 mm for cc7a- and cc7b-named specimens.

The outer steel tube yield strength, diameter, and thickness for C1-1- and C1-2-named CFDST column specimens obtained from the study of Han et al. [29] were 319.6 MPa, 220 mm, and 3.62 mm, respectively; whereas the inner steel tube of both specimens had the yield strength of 380.6 MPa, the diameter of 159 mm, and thickness of 3.72 mm. The compressive strengths of the samples were 48 MPa and their lengths were 660 mm.

Furthermore, 0HA0- and 0HB0-designated samples from the study of Wang et al. [30] were chosen to verify the FEM model. The yield strengths of both outer and inner steel tubes were the same for both specimens and it was 350 MPa. The diameters and thicknesses of the outer steel tube for both specimens were 165 mm and 1.7 mm, respectively. The concrete compressive strengths and the lengths of both specimens were 28.1 MPa and 500 mm, respectively. The differentness between 0HA0 and 0HB0 denoted specimens was in the inner steel tube diameter and thickness. The inner steel tube diameter and thickness of the 0HA0-labeled specimen were 76 mm and 1.2 mm, respectively; while they were 114 mm and 1.7 mm for 0HB0-labeled specimen, respectively.

Moreover, two CFDST column specimens, one from the study of Lu et al. [31] and another from the study of Wang et al. [32], were used to confirm the FEM model. The C2-C4-SCC1-Ref-named specimen from the study of Lu et al. [31] had the outer and inner steel tube yield strengths of 426 MPa. The diameter and thickness values for the outer steel tube were 219.1 mm and 5 mm, respectively, and for the inner steel tube 101.6 mm and 3.2 mm, respectively. The concrete with a compressive strength of 46.6 MPa was utilized in the manufacturing of the specimen and the length

of the specimen was 800 mm. On the other hand, the CFDST columns specimen with label of ACI140x3-HC38X8-C80 from the study of Wang et al. [32] had the outer steel tube yield strength, diameter, and thickness values of 300 MPa, 140.1 mm, and 2.9 mm, respectively, and the inner steel tube yield strength, diameter and thickness values of 433 MPa, 38 mm, and 7.51 mm, respectively. The specimen was manufactured using the concrete with a compressive strength of 79.9 MPa and the length of the specimen was 350 mm.

In total, 14 CFDST column specimens with CHS were used to verify and calibrate the proposed FEM model. These specimens were chosen according to the specifications of the CFDST columns stated in the parametric study part. The aforementioned properties of the CFDST column specimens are also presented in Table 1.

The predicted ultimate axial strength and normalized results of the FEM model are tabulated in Table 2. The results indicated that the proposed FEM model predicts the ultimate axial strength near the experimental test values. The average normalized ultimate axial strength value of 1.037 and the coefficient of variation value of 0.093 were obtained by the prediction of the FEM model. In addition, the prediction performance of the model was statistically evaluated by means of mean absolute percent error (MAPE), mean square error (MSE), and root mean square error (RMSE) values. The MAPE, MSE, and RMSE were calculated using Eqs. 23, 24, and 25, respectively. Table 2 also includes the MAPE, MSE, and RMSE values. By the FEM model, the error values of 7.22, 32,115, and 127.5 were achieved for the

MAPE, MSE, and RMSE, respectively. These error values also affirm that the proposed FEM model has a good prediction capability and it estimates reliable and accurate ultimate axial strengths.

$$\text{MAPE} = \frac{1}{n} \sum_{i=1}^{n} \left| \frac{m_i - p_i}{m_i} \right| \times 100, \tag{23}$$

$$\text{MSE} = \frac{\sum_{i=1}^{n} (m_i - p_i)^2}{n}, \tag{24}$$

$$\text{RMSE} = \sqrt{\frac{\sum_{i=1}^{n} (m_i - p_i)^2}{n}}, \tag{25}$$

where m and p are the values of measured (m_i) and the predicted (p_i) values, respectively.

Moreover, the load–displacement and load–strain curves procured from the FEM model were also compared with that attained from the experiment. Figure 9a, b indicates the comparison of the experimental load–displacement curves of the C1C7 sample from the study of Zhao et al. [27] and C2-C4-SCC1-Ref sample from the study of Lu et al. [31], respectively, with the curves achieved from the proposed FEM model.

Besides, Fig. 10a, b demonstrates the comparison of the experimental load–strain curves of the cc4b sample from the study of Tao et al. [28] and the 0HA0 sample from the

Table 1 Experimental dataset used in the verification of model

References	Sample ID	Yield strength		Diameter		Thickness		Concrete compressive strength, f_c' (MPa)	Length of specimen, L (mm)
		Outer steel tube, f_{syo} (MPa)	Inner steel tube, f_{syi} (MPa)	Outer steel tube, D_o (mm)	Inner steel tube, D_i (mm)	Outer steel tube, t_o (mm)	Inner steel tube, t_i (mm)		
Uenaka et al. [2]	c16-1125	308.0	308.0	158.0	114.0	1.50	1.50	18.7	450
	c23-1125	286.0	286.0	157.0	115.0	2.14	2.14	18.7	450
Zhao et al. [27]	C1C7	454.0	425.0	114.5	48.4	2.80	5.90	63.4	400
	C2C7	416.0	425.0	114.6	48.4	2.80	4.70	63.4	400
Tao et al. [28]	cc4a	275.9	342.0	180.0	48.0	3.00	3.00	40.0	540
	cc4b	275.9	342.0	180.0	48.0	3.00	3.00	40.0	540
	cc7a	275.9	320.5	300.0	165.0	3.00	3.00	40.0	900
	cc7b	275.9	320.5	300.0	165.0	3.00	3.00	40.0	900
Han et al. [29]	C1-1	319.6	380.6	220.0	159.0	3.62	3.72	60.0	660
	C1-2	319.6	380.6	220.0	159.0	3.62	3.72	60.0	660
Wang et al. [30]	0HA0	350.0	350.0	165.0	76.0	1.70	1.20	28.1	500
	0HB0	350.0	350.0	165.0	114.0	1.70	1.70	28.1	500
Lu et al. [31]	C2-C4-SCC1-Ref	426.0	426.0	219.1	101.6	5.00	3.20	46.6	800
Wang et al. [32]	ACI140x3-HC38X8-C80	300.0	433.0	140.1	38.0	2.90	7.51	79.9	350

Table 2 Prediction performance of the proposed FEM model

References	Sample ID	$P_{u,exp}$ (kN)	Average	$P_{u,FEM}$ (kN)	$P_{u,exp}/P_{u,FEM}$
Uenaka et al. [2]	c16-1125	589.0		598.1	0.98
	c23-1125	703.6		752.8	0.93
Zhao et al. [27]	C1C7	1415.0		1444.0	0.98
	C2C7	1380.0		1326.0	1.04
Tao et al. [28]	cc4a	1435.0	1396.5	1413.0	0.99
	cc4b	1358.0			
	cc7a	3331.0	3298.5	2872.0	1.15
	cc7b	3266.0			
Han et al. [29]	C1-1	2537.0	2551.5	2323.0	1.10
	C1-2	2566.0			
Wang et al. [30]	0HA0	980.0		820.8	1.19
	0HB0	715.0		785.4	0.91
Lu et al. [31]	C2-C4-SCC1-Ref	3333.0		3420.0	0.97
Wang et al. [32]	ACI140x3-HC38X8-C80	2083.4		1810.0	1.15
Ave					1.037
COV					0.093
MAPE				7.22	
MSE				32,115	
RMSE				127.5	

Ave average of normalized ultimate axial strengths, *COV* coefficient of variation, *MAPE* mean absolute percent error, *MSE* mean square error, *RMSE* root mean square error

(a)

(b)
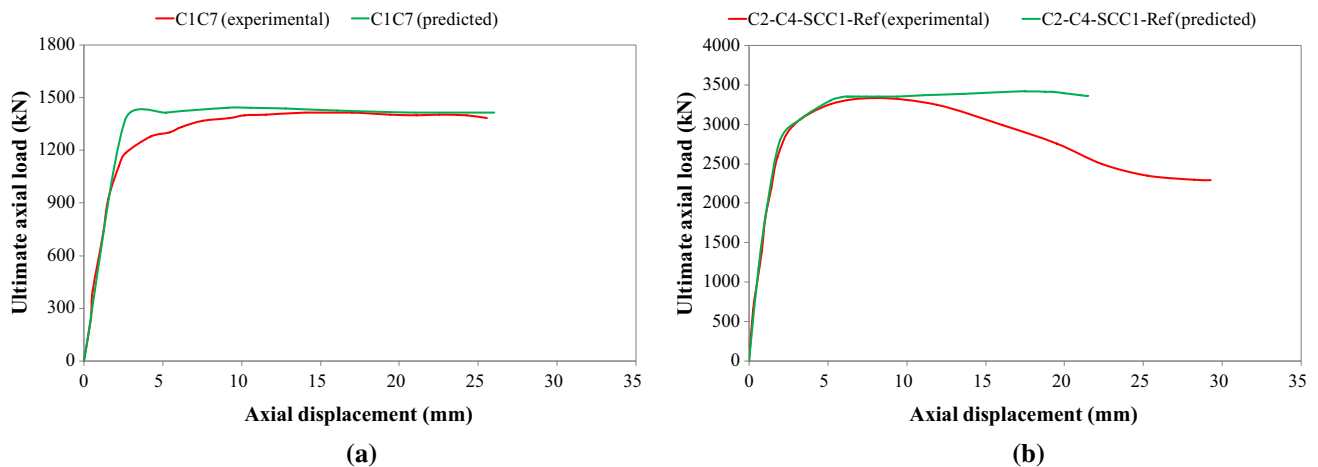
Fig. 9 Comparison of the experimental and FEM results on the load vs. displacement curves of: **a** C1C7 sample [27] and **b** C2-C4-SCC1-Ref sample [31]

study of Wang et al. [30], respectively, with the curves, achieved from the proposed FEM model. According to the load–displacement and load–strain curves, it can be absolutely stated that the FEM model has a very well prediction performance, in particular, the axial stiffness of the CFDST columns with CHS. Additionally, it can be specified about the proposed FEM model that it estimates robust and reliable ultimate axial strength values and acceptable post-peak behaviors.

5 Parametric study

The study herein was aimed to model various CFDST columns with CHS using the verified FEM model. Therefore, 72 CFDST columns with CHS were designed in ABAQUS CAE [32] to identify the effectiveness of parameters on the ultimate axial strength of such columns. In these columns, the length (L) of specimen and yield strengths of outer
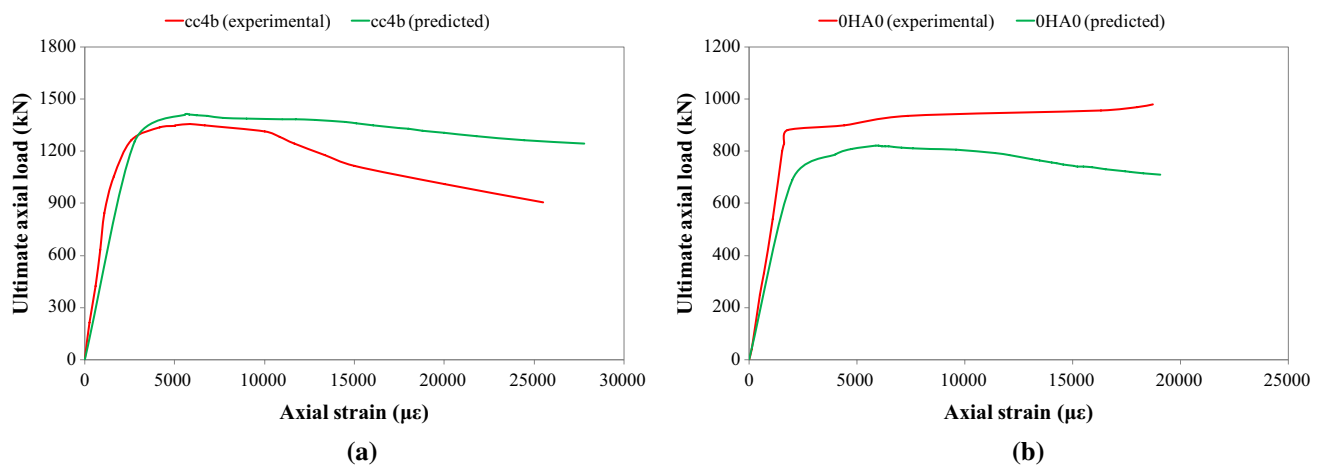
Fig. 10 Comparison of the experimental and FEM results on the load vs. strain curves of **a** cc4b sample [28] and **b** 0HA0 sample [30]

(f_{syo}) and inner (f_{syi}) steel tubes were kept constant; while the diameters (D_o and D_i) and thicknesses (t_o and t_i) of outer and inner steel tubes and the compressive strength of the concrete annulus (f_c') were the variable parameters. Two outer steel tube diameters with values of 200 and 300 mm, three different outer steel tube thicknesses with values of 2, 3, and 4 mm, two inner steel tube diameters with values of 80 and 120 mm, and three different inner steel tube thicknesses with values of 1, 2, and 3 mm were chosen to investigate and visualize the effect of sectional properties of CFDST columns with CHS. By changing the outer steel tube diameter with keeping the length of specimen constant, mainly L/D_o ratio has been changed. In addition to examining the sectional properties, two different concrete compressive strength with values of 25 and 50 MPa were considered in the designing of columns to reveal the effect of concrete compressive strength on the ultimate axial strength of CFDST columns. According to these parameters, in total, 72 different columns were designed. The detail of each column used in this parametric study is presented in Table 3.

Each CFDST column specimen was designed according to the specifications given in Sect. 2. The ultimate axial strength of each specimen was predicted after designing using ABAQUS CAE [36] software. The ultimate axial strength values predicted by the proposed FEM model are tabulated in Table 4. According to these results, Figs. 11a, b, 12a, b are plotted.

The ultimate axial strength predicted by the FEM model versus the outer steel tube thickness is given in Fig. 11a, b in the case of $L/D_o = 3$ and $L/D_o = 2$, respectively. These figures also include the variation in the ultimate axial strength regarding both inner steel tube thickness and concrete compressive strength. It can be clearly seen from Fig. 11a, b that increasing both outer and inner steel tubes thicknesses

results in the increment of the ultimate axial strength. In the case of $L/D_o = 3$, $D_i = 80$ mm, and $f_c' = 25$ MPa, increasing the outer steel tube thickness from 2 to 4 mm results in 48, 46, and 44% increment of the ultimate axial strength when the inner steel tube thicknesses are 1, 2, and 3 mm, respectively. When the L/Do ratio is decreased from 3 to 2, these increment rates in the ultimate axial strength are 39, 38, and 37% when the inner steel tube thicknesses are 1, 2, and 3 mm, respectively. The results also indicate that when the L/Do ratio is decreased from 3 to 2, namely when the diameter of the outer steel tube is increased without changing the length of the specimen, the remarkable enhancement in the ultimate axial strength is observed. Another finding is that using concrete with higher compressive strength significantly increases the ultimate axial strength of the CFDST columns. In the case of $L/D_o = 3$, $D_i = 80$ mm, and $f_c' = 50$ MPa, increasing the outer steel tube thickness from 2 to 4 mm results in 24, 23, and 22% increase of the ultimate axial strength when the inner steel tube thicknesses are 1, 2, and 3 mm, respectively. When the L/Do ratio is decreased from 3 to 2, these increment rates in the ultimate axial strength are 23, 22, and 22% when the inner steel tube thicknesses are 1, 2, and 3 mm, respectively.

Another changeable parameter is the diameter of the inner steel tube (D_i). Figure 12a, b demonstrate the predicted ultimate axial strength of the CFDST columns according to the outer steel tube thickness when the D_i is 120 mm and other parameters are the same as in Fig. 11a, b. The results show that increasing the D_i from 80 to 120 mm decreases the load-carrying capacity of the CFDST columns. The effect of the concrete compressive strength can also be observed when the D_i is 120 mm. The higher compressive strength means the higher ultimate axial strength of the CFDST columns. Besides, when Fig. 12a, b are examined, it can be obviously seen that increasing the diameter of the outer steel tube (D_o)

Table 3 Properties of the CFDST columns used in the parametric study

Sample no	Yield strength		Diameter		Thickness		Concrete compressive strength, f_c' (MPa)	Length of specimen, L (mm)
	Outer steel tube, f_{syo} (MPa)	Inner steel tube, f_{syi} (MPa)	Outer steel tube, D_o (mm)	Inner steel tube, D_i (mm)	Outer steel tube, t_o (mm)	Inner steel tube, t_i (mm)		
1	365	365	200	80	2	1	25	600
2	365	365	200	80	2	2	25	600
3	365	365	200	80	2	3	25	600
4	365	365	200	80	3	1	25	600
5	365	365	200	80	3	2	25	600
6	365	365	200	80	3	3	25	600
7	365	365	200	80	4	1	25	600
8	365	365	200	80	4	2	25	600
9	365	365	200	80	4	3	25	600
10	365	365	200	120	2	1	25	600
11	365	365	200	120	2	2	25	600
12	365	365	200	120	2	3	25	600
13	365	365	200	120	3	1	25	600
14	365	365	200	120	3	2	25	600
15	365	365	200	120	3	3	25	600
16	365	365	200	120	4	1	25	600
17	365	365	200	120	4	2	25	600
18	365	365	200	120	4	3	25	600
19	365	365	300	80	2	1	25	600
20	365	365	300	80	2	2	25	600
21	365	365	300	80	2	3	25	600
22	365	365	300	80	3	1	25	600
23	365	365	300	80	3	2	25	600
24	365	365	300	80	3	3	25	600
25	365	365	300	80	4	1	25	600
26	365	365	300	80	4	2	25	600
27	365	365	300	80	4	3	25	600
28	365	365	300	120	2	1	25	600
29	365	365	300	120	2	2	25	600
30	365	365	300	120	2	3	25	600
31	365	365	300	120	3	1	25	600
32	365	365	300	120	3	2	25	600
33	365	365	300	120	3	3	25	600
34	365	365	300	120	4	1	25	600
35	365	365	300	120	4	2	25	600
36	365	365	300	120	4	3	25	600
37	365	365	200	80	2	1	50	600
38	365	365	200	80	2	2	50	600
39	365	365	200	80	2	3	50	600
40	365	365	200	80	3	1	50	600
41	365	365	200	80	3	2	50	600
42	365	365	200	80	3	3	50	600
43	365	365	200	80	4	1	50	600
44	365	365	200	80	4	2	50	600
45	365	365	200	80	4	3	50	600
46	365	365	200	120	2	1	50	600
47	365	365	200	120	2	2	50	600

Table 3 (continued)

Sample no	Yield strength		Diameter		Thickness		Concrete compressive strength, f_c' (MPa)	Length of specimen, L (mm)
	Outer steel tube, f_{syo} (MPa)	Inner steel tube, f_{syi} (MPa)	Outer steel tube, D_o (mm)	Inner steel tube, D_i (mm)	Outer steel tube, t_o (mm)	Inner steel tube, t_i (mm)		
48	365	365	200	120	2	3	50	600
49	365	365	200	120	3	1	50	600
50	365	365	200	120	3	2	50	600
51	365	365	200	120	3	3	50	600
52	365	365	200	120	4	1	50	600
53	365	365	200	120	4	2	50	600
54	365	365	200	120	4	3	50	600
55	365	365	300	80	2	1	50	600
56	365	365	300	80	2	2	50	600
57	365	365	300	80	2	3	50	600
58	365	365	300	80	3	1	50	600
59	365	365	300	80	3	2	50	600
60	365	365	300	80	3	3	50	600
61	365	365	300	80	4	1	50	600
62	365	365	300	80	4	2	50	600
63	365	365	300	80	4	3	50	600
64	365	365	300	120	2	1	50	600
65	365	365	300	120	2	2	50	600
66	365	365	300	120	2	3	50	600
67	365	365	300	120	3	1	50	600
68	365	365	300	120	3	2	50	600
69	365	365	300	120	3	3	50	600
70	365	365	300	120	4	1	50	600
71	365	365	300	120	4	2	50	600
72	365	365	300	120	4	3	50	600

from 200 to 300 mm by keeping the length of specimen constant results in the doubling of the load-carrying capacity of the CFDST columns.

When Figs. 11a, b, 12a, b are considered, it can be obviously seen that increasing the inner steel tube thickness is not effective on the ultimate axial strength as much as increasing the outer steel tube thickness. The increment rates in the ultimate axial strength by increasing the outer steel tube thickness are in the range of 37–52% and 22–29% in the case of $f_c' = 25$ and 50 MPa, respectively; whereas when the thickness of the inner steel tube is increased, the increment percentages in the ultimate axial strength are between 5 and 24%, and 3 and 17% for $f_c' = 25$ and 50 MPa, respectively.

To clearly indicate the change in the ultimate axial strength of the CFDST columns with regard to altering of L/D_o, D_i, t_o, t_i, and f_c', Fig. 13a, b is plotted. It can be stated that the slight increase in the ultimate axial strength can be seen when the inner steel tube thickness is increased, while a significant enhancement in the load-carrying capacity of CFDST columns can be observed

when the outer steel tube thickness is increased. Besides, it is obvious that the most significant increase in the ultimate axial strength is seen when the L/D_o is reduced or D_o is increased and the compressive strength of the concrete annulus is increased.

The similar findings of the ultimate axial strength regarding the change in such properties can be found in the experimental studies available in the literature. For example, Uenaka et al. [2] investigated the influences of diameter and yield strength of the outer steel tube and the diameter and thickness of the inner steel tube. In this experimental study, the diameter of the inner steel tube of some specimens was increased from 39 to 77 mm and then from 77 to 114 mm by keeping the other parameters constant, the gradual decreasing in the ultimate axial strength was observed. But the individual effect of other changeable parameters could not be explained since three of them were altered with together.

In the experimental study of Zhao et al. [27], in two CFDST column specimens, the individual effect of inner steel

Table 4 Comparison of the ultimate axial strengths predicted by FEM model with modified and proposed formulas

| Sample no.	$P_{u,FEM}$ (kN)	$P_{u,FEM}/P_{u,ACI}$	$P_{u,FEM}/P_{u,EC4}$	$P_{u,FEM}/P_{u,AISC}$	$P_{u,FEM}/P_{u,Uenaka\ et\ al.}$	$P_{u,FEM}/P_{u,Han\ et\ al.}$	$P_{u,FEM}/P_{u,Yu\ et\ al.}$	$P_{u,FEM}/P_{u,Hassanein\ et\ al.}$
1	1288	1.19	0.91	1.13	0.83	1.08	1.02	1.10
2	1374	1.18	0.92	1.12	0.84	1.07	1.02	1.08
3	1461	1.17	0.94	1.11	0.85	1.07	1.02	1.07
4	1584	1.23	0.91	1.18	0.82	1.10	1.01	1.11
5	1679	1.22	0.93	1.17	0.83	1.10	1.02	1.10
6	1772	1.21	0.95	1.17	0.84	1.10	1.02	1.09
7	1909	1.27	0.93	1.23	0.82	1.13	1.03	1.14
8	2008	1.27	0.95	1.22	0.83	1.13	1.03	1.13
9	2105	1.26	0.96	1.22	0.84	1.13	1.03	1.13
10	1156	1.17	0.95	1.12	0.96	1.07	1.03	1.11
11	1295	1.15	0.98	1.11	0.97	1.07	1.03	1.09
12	1439	1.14	1.00	1.11	0.98	1.07	1.03	1.08
13	1463	1.22	0.98	1.18	0.99	1.11	1.04	1.13
14	1615	1.21	1.01	1.17	1.00	1.12	1.05	1.13
15	1763	1.20	1.03	1.17	1.01	1.12	1.05	1.12
16	1759	1.25	0.99	1.21	1.00	1.13	1.05	1.15
17	1906	1.23	1.02	1.20	1.01	1.13	1.05	1.14
18	2059	1.23	1.04	1.20	1.02	1.13	1.06	1.14
19	2469	1.16	0.84	1.08	0.78	1.04	1.02	1.15
20	2556	1.15	0.85	1.08	0.78	1.04	1.02	1.14
21	2642	1.15	0.86	1.07	0.79	1.04	1.02	1.13
22	2993	1.22	0.86	1.15	0.77	1.10	1.03	1.14
23	3079	1.21	0.87	1.14	0.78	1.09	1.03	1.13
24	3165	1.21	0.88	1.14	0.78	1.09	1.03	1.12
25	3429	1.24	0.85	1.18	0.75	1.10	1.02	1.13
26	3521	1.23	0.86	1.17	0.75	1.10	1.02	1.13
27	3613	1.23	0.87	1.17	0.76	1.10	1.02	1.12
28	2351	1.15	0.86	1.08	0.83	1.04	1.02	1.15
29	2495	1.15	0.88	1.08	0.84	1.04	1.02	1.14
30	2627	1.14	0.89	1.07	0.85	1.04	1.02	1.13
31	2854	1.21	0.87	1.14	0.84	1.09	1.03	1.14
32	2992	1.20	0.89	1.14	0.84	1.09	1.03	1.13
33	3127	1.19	0.90	1.13	0.85	1.08	1.03	1.12
34	3298	1.23	0.87	1.17	0.82	1.11	1.02	1.14
35	3452	1.23	0.89	1.17	0.83	1.11	1.03	1.14
36	3601	1.22	0.90	1.17	0.84	1.11	1.03	1.13
37	1906	1.18	0.93	1.10	0.88	1.05	1.07	1.09
38	1992	1.17	0.94	1.10	0.88	1.04	1.06	1.08
39	2078	1.16	0.95	1.09	0.88	1.04	1.06	1.07
40	2150	1.19	0.91	1.12	0.84	1.04	1.04	1.08
41	2237	1.18	0.92	1.11	0.85	1.04	1.03	1.07
42	2323	1.17	0.93	1.11	0.85	1.04	1.03	1.06
43	2368	1.18	0.89	1.12	0.81	1.03	1.00	1.07
44	2456	1.17	0.90	1.11	0.81	1.02	1.00	1.06
45	2542	1.17	0.91	1.11	0.82	1.02	1.00	1.05
46	1607	1.15	0.95	1.09	0.96	1.04	1.06	1.09
47	1742	1.14	0.96	1.08	0.96	1.04	1.05	1.08
48	1874	1.13	0.98	1.07	0.97	1.03	1.05	1.07
49	1855	1.17	0.95	1.11	0.96	1.04	1.04	1.09
50	1989	1.15	0.96	1.10	0.96	1.04	1.04	1.08
51	2121	1.14	0.98	1.09	0.96	1.04	1.03	1.07
52	2070	1.16	0.93	1.11	0.94	1.03	1.01	1.07
53	2217	1.16	0.95	1.11	0.95	1.04	1.02	1.07
54	2367	1.15	0.98	1.11	0.96	1.04	1.02	1.07
55	4013	1.15	0.88	1.06	0.84	1.02	1.07	1.14

Table 4 (continued)

Sample no.	$P_{u,FEM}$ (kN)	$P_{u,FEM}/P_{u,ACI}$	$P_{u,FEM}/P_{u,EC4}$	$P_{u,FEM}/P_{u,AISC}$	$P_{u,FEM}/P_{u,Uenaka\ et\ al.}$	$P_{u,FEM}/P_{u,Han\ et\ al.}$	$P_{u,FEM}/P_{u,Yu\ et\ al.}$	$P_{u,FEM}/P_{u,Hassanein\ et\ al.}$
56	4100	1.15	0.88	1.06	0.85	1.02	1.06	1.13
57	4185	1.14	0.89	1.05	0.85	1.02	1.06	1.13
58	4530	1.20	0.89	1.11	0.83	1.05	1.07	1.14
59	4617	1.19	0.90	1.11	0.83	1.05	1.07	1.13
60	4686	1.18	0.90	1.10	0.83	1.05	1.07	1.12
61	4924	1.21	0.88	1.12	0.80	1.06	1.05	1.13
62	5012	1.20	0.88	1.12	0.81	1.05	1.05	1.12
63	5098	1.20	0.89	1.12	0.81	1.05	1.05	1.12
64	3743	1.15	0.89	1.06	0.88	1.02	1.07	1.14
65	3877	1.14	0.90	1.05	0.88	1.02	1.06	1.13
66	4009	1.14	0.90	1.05	0.89	1.02	1.06	1.12
67	4249	1.19	0.90	1.11	0.88	1.06	1.07	1.14
68	4382	1.19	0.91	1.10	0.88	1.05	1.07	1.14
69	4514	1.18	0.92	1.10	0.89	1.05	1.07	1.13
70	4632	1.20	0.89	1.12	0.86	1.06	1.06	1.13
71	4766	1.19	0.90	1.12	0.86	1.05	1.05	1.12
72	4898	1.19	0.91	1.11	0.87	1.05	1.05	1.12
Ave		1.19	0.92	1.12	0.87	1.07	1.04	1.11
COV		0.029	0.049	0.039	0.082	0.032	0.019	0.025
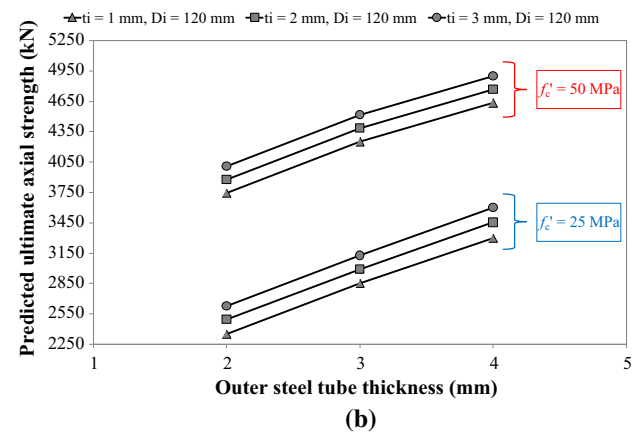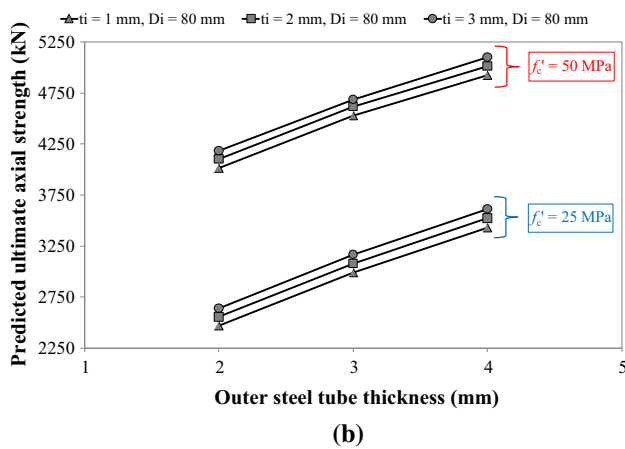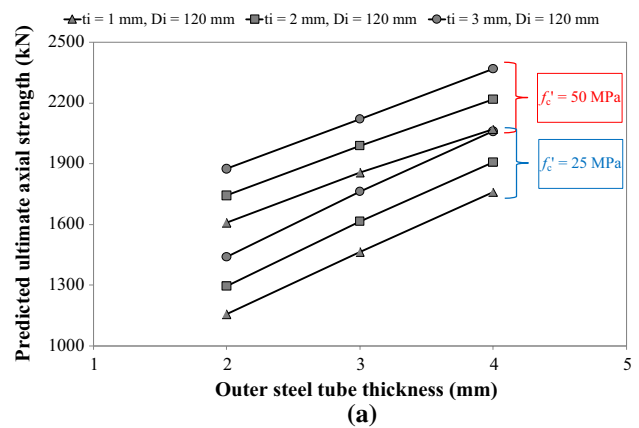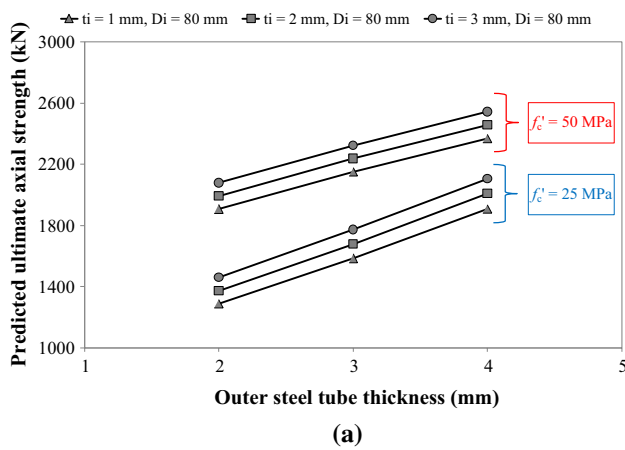
Fig. 11 Ultimate axial strength predicted by FEM model vs. outer steel tube thickness for: **a** $L/D_o = 3$, $D_i = 80$ mm and **b** $L/D_o = 2$, $D_i = 80$ mm
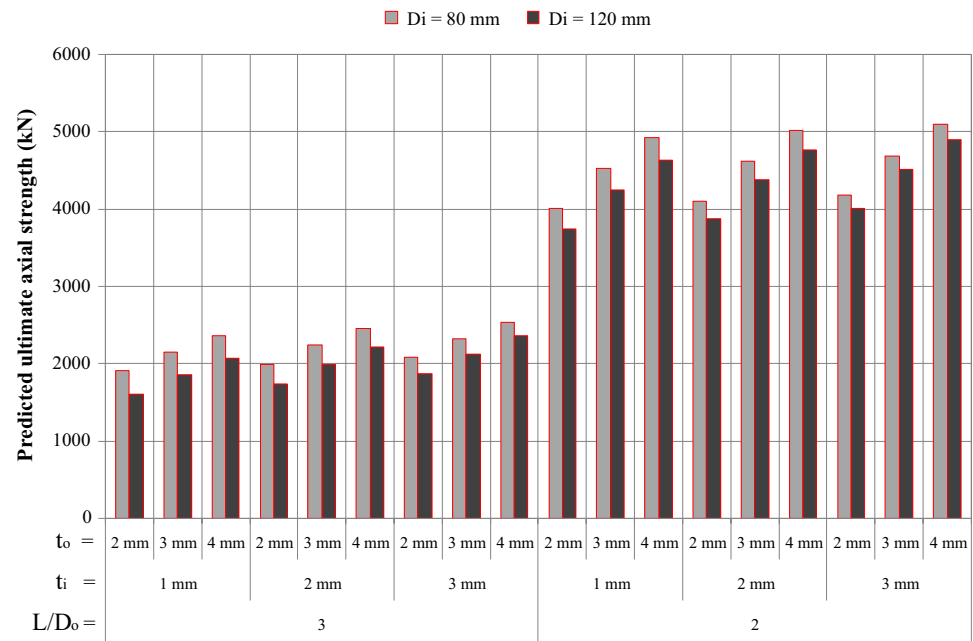

Fig. 12 Ultimate axial strength predicted by FEM model vs. outer steel tube thickness for: **a** $L/D_o = 3$, $D_i = 120$ mm and **b** $L/D_o = 2$, $D_i = 120$ mm

Fig. 13 Variation in ultimate axial strength predicted by FEM model with regard to L/D_o, D_i, t_o, t_i values in the case of: **a** $f_c' = 25$ MPa and **b** $f_c' = 50$ MPa
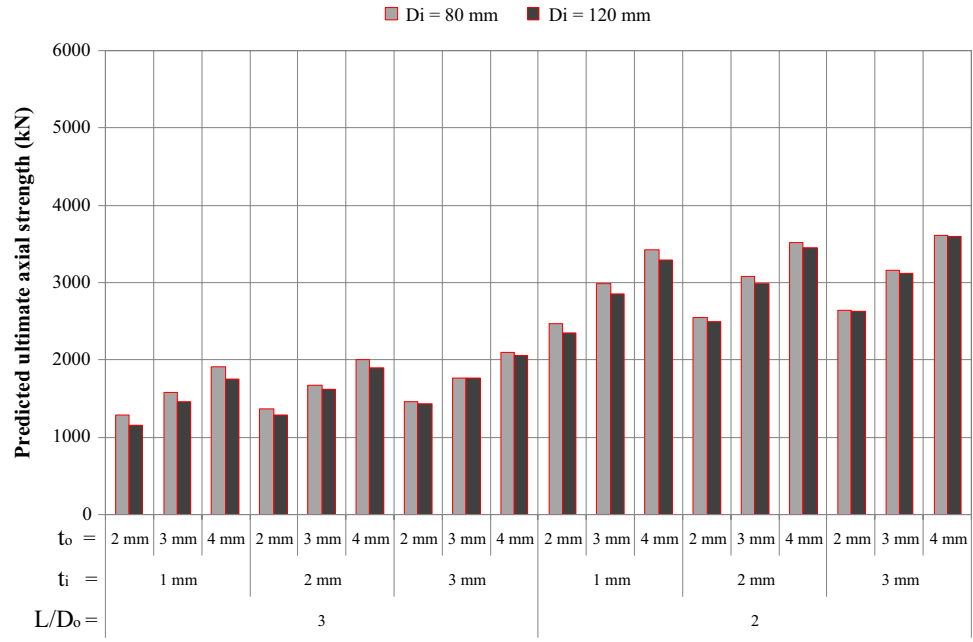
(a)

(b)

tube thickness could be comprehended. In these two specimens, the diameter of outer steel tube, inner steel tube yield strength and diameter, length of specimen, and concrete compressive strength were constant; whereas, the yield strength and diameter of outer steel tube were 454 MPa and 114.5 mm for one specimen, respectively, and 453 MPa and 114.4 mm for other specimen, respectively. The variation in the yield strength and diameter of the outer steel tube could be negligible and accepted as constant. In this situation, the only

changeable parameter was the thickness of the inner steel tube and it was 5.9 mm for the first specimen and 3.5 mm for the second one. This means that the inner steel tube thickness was decreased from 5.9 to 3.5 mm, which resulted in the reducing of the ultimate axial strength.

In another study of Zhao et al. [60], in two CFDST column specimens, all parameters were kept constant except the thickness of the outer steel tube, which was 6.0 mm for one sample and 3.6 mm for another sample. The CFDST column specimen

manufactured with a 6-mm outer steel tube performed higher ultimate axial strength than that produced with a 3.6-mm outer steel tube. Namely, increasing the outer steel tube diameter enhanced the load-carrying capacity of the CFDST columns. A similar result was found in the study of Lin and Tsai [61]: the thickness of outer steel tube was increased from 2 to 4 mm with keeping the other properties constant and the increase in the ultimate axial strength was observed.

In addition, in the study of Han et al. [50], the effect of inner steel tube diameter was investigated and it was revealed that reducing the inner steel tube from 159 to 106 mm significantly increased the ultimate axial strength of CFDST columns. This situation was also observed in the experimental study of Dong and Ho [62]. The inner steel tube diameter with the values of 88.9 and 114.3 mm was used in the manufacturing of the CFDST column specimen. In this study, it was found out that the lower diameter of the inner steel tube resulted in higher ultimate axial strength. Besides, Dong and Ho [62] investigated the effect of concrete compressive strength in the same study. Two concrete compressive strength grades of 50 and 85 MPa were chosen in their study. The CFDST column specimen manufactured with concrete having higher compressive strength ensued to higher load-carrying capacity. The similar results were also found in the study of Han et al. [29] and Wang et al. [30]. The experimental programs of Han et al. [29] and Wang et al. [30] were conducted using two concrete compressive strength values of 39.3–66.4 MPa and 40.5–79.9 MPa, respectively, and it was revealed that the specimens manufactured using the concrete having higher compressive strength performed higher ultimate axial strength values.

Besides, the ultimate axial strength of these CFDST columns specimens was estimated using the formulas modified from ACI [39], EC4 [48], and AISC [49] as well as the empirical models suggested by Uenaka et al. [2], Han et al. [50], Yu et al. [51], and Hassanein et al. [52]. The normalized ultimate axial strength values with respect to the proposed FEM model are also presented in Table 4. The normalized results indicate that the formula modified from EC4 [48] and the empirical model suggested by Uenaka et al. [2] have generally overestimated ultimate axial strength values with respect to the proposed FEM model; whereas, the other modified formulas and the suggested empirical models have the underestimated values.

6 Statistical evaluation of models

The effects of independent parameters such as the diameters and thicknesses of outer and inner steel tubes and the compressive strength of concrete annulus are graphically illustrated in the previous section. Here, the results are statistically evaluated. For this, the analysis of variance (ANOVA) was used to indicate the effectiveness of independent variables on the dependent variable. The analysis method known as general linear model analysis of variance (GLM-ANOVA) was utilized in the statistical evaluation of the results. The software named "Minitab" including the GLM-ANOVA method was employed in performing the statistical analysis [63]. The GLM-ANOVA is a diagnostic tool that decreases the control variance to help a control factor dominance to be quantified.

In this study, the diameter and thickness of the outer and inner steel tubes and the concrete compressive strength were designated as the independent variables while the ultimate axial strength of the double skin composite columns was identified as the dependent variable. Besides, the significance level of 0.05 was adjusted in the analysis to reveal which independent variable is a statistically important parameter on the dependent variable. The results obtained from the statistical analysis of the proposed FEM model are presented in Table 5. The significance of the independent parameters can be comprehended taking into consideration the P values. If the P value of any independent variable is greater than the level of significance, it can be stated that this variable has an insignificant effect on the dependent variable. On the contrary case, namely, when the P value of any independent variable is less than the level of significance, it can be incontrovertibly specified that this parameter can be approved as a significant variable on the dependent variable. The statistical analysis results show that all independent variables have a significant effect on the ultimate axial strength of the CFDST columns since the P values of each independent variable is less than the significance level value of 0.05. Even though all independent variables are statistically significant parameters on the ultimate axial strength, it should be also stated the degree of effectiveness of each independent variable. Therefore, the contributions of the independent variables on the ultimate axial strength of the CFDST columns are given as percentages under the last column in Table 5. The higher percent contribution of the independent variable implies the higher effectiveness of this variable on the dependent variable. According to the percent contribution values presented in Table 5, it can be easily said that the most significant parameter that affects the ultimate axial strength of the CFDST columns is the diameter of the outer steel tube. However, the influences of inner steel tube diameter and thickness can be accepted as negligible since their percent contributions values are too small when they are compared with the percent contributions of the outer steel tube diameter and the concrete compressive strength. The second most significant independent variable is the concrete compressive strength with the percent contribution value of 17.8 and the effectiveness

Table 5 Statistical analysis of the ultimate axial strength of the CFDST columns predicted by the proposed FEM model, modified code formulas, and empirical models suggested by the previous researchers

Dependent variable	Independent variable	Sequential sum of squares	Computed F	P value	Significance	Contribution (%)
$P_{u,FEM}$	D_o	62,291,401	796.5	0.000	Yes	68.3
	D_i	451,250	5.8	0.019	Yes	0.5
	t_o	6,559,575	41.9	0.000	Yes	7.2
	t_i	623,141	4.0	0.023	Yes	0.7
	f_c'	16,273,513	208.1	0.000	Yes	17.8
	Error	5,005,538	–	–	–	5.5
	Total	91,204,418	–	–	–	–
$P_{u,ACI}$ [39]	D_o	44,125,003	875.6	0.000	Yes	68.3
	D_i	212,065	4.2	0.044	Yes	0.3
	t_o	3,129,951	31.1	0.000	Yes	4.8
	t_i	581,681	5.8	0.005	Yes	0.9
	f_c'	13,369,654	265.3	0.000	Yes	20.7
	Error	3,225,253	–	–	–	5.0
	Total	64,643,606	–	–	–	–
$P_{u,EC4}$ [48]	D_o	90,973,095	1114.9	0.000	Yes	72.9
	D_i	1,285,030	15.8	0.000	Yes	1.0
	t_o	7,757,532	47.5	0.000	Yes	6.2
	t_i	357,543	2.2	0.120	No	0.3
	f_c'	19,250,582	235.9	0.000	Yes	15.4
	Error	5,222,113	–	–	–	4.2
	Total	124,845,896	–	–	–	–
$P_{u,AISC}$ [49]	D_o	52,590,321	846.5	0.000	Yes	68.2
	D_i	310,064	5.0	0.029	Yes	0.4
	t_o	3,053,361	24.6	0.000	Yes	4.0
	t_i	576,206	4.6	0.013	Yes	0.7
	f_c'	16,579,958	266.9	0.000	Yes	21.5
	Error	3,975,930	–	–	–	5.2
	Total	77,085,841	–	–	–	–
$P_{u,Uenaka\ et\ al.}$ [2]	D_o	105,097,136	1198.9	0.000	Yes	72.3
	D_i	4,419,162	50.4	0.000	Yes	3.0
	t_o	11,146,467	63.6	0.000	Yes	7.7
	t_i	581,681	3.3	0.043	Yes	0.4
	f_c'	18,504,712	221.1	0.000	Yes	12.7
	Error	5,610,553	–	–	–	3.9
	Total	145,359,710	–	–	–	–
$P_{u,Han\ et\ al.}$ [50]	D_o	56,482,401	838.1	0.000	Yes	66.7
	D_i	429,846	6.4	0.014	Yes	0.5
	t_o	4,385,363	32.5	0.000	Yes	5.2
	t_i	581,681	4.3	0.017	Yes	0.7
	f_c'	18,485,030	274.3	0.000	Yes	21.8
	Error	4,313,366	–	–	–	5.1
	Total	84,677,687	–	–	–	–
$P_{u,Yu\ et\ al.}$ [51]	D_o	55,256,666	1048.0	0.000	Yes	69.8
	D_i	492,636	9.3	0.003	Yes	0.6
	t_o	6,525,680	61.9	0.000	Yes	8.2
	t_i	581,681	5.5	0.006	Yes	0.7
	f_c'	12,979,321	246.2	0.000	Yes	16.4
	Error	3,374,412	–	–	–	4.3
	Total	79,210,396	–	–	–	–

Table 5 (continued)

Dependent variable	Independent variable	Sequential sum of squares	Computed F	P value	Significance	Contribution (%)
$P_{\text{u,Hassanein et al.}}$ [52]	D_o	45,195,453	855.6	0.000	Yes	65.5
	D_i	427,649	8.1	0.006	Yes	0.6
	t_o	5,291,356	50.1	0.000	Yes	7.7
	t_i	678,137	6.4	0.003	Yes	1.0
	f_c'	14,069,778	266.4	0.000	Yes	20.4
	Error	3,380,654	–	–	–	4.9
	Total	69,043,026	–	–	–	–

D_o diameter of outer steel tube, D_i diameter of inner steel tube, t_o thickness of outer steel tube, t_i thickness of inner steel tube, f_c' concrete compressive strength

of the outer steel tube thickness can be approved as moderate due to having a 7.2% contribution value.

The statistical analysis of the ultimate axial strength results achieved using the proposed FEM model indicates that all independent parameters, namely, the diameter and the thickness of the outer and inner steel tubes and the concrete compressive strength, are the significant parameters in the determination of the ultimate axial strength of the CFDST columns according to the P values, but the most significant parameter is the diameter of the outer steel tube and the lowest significant parameter can be accepted as the diameter and thickness of the inner steel tube regarding the percent contribution values.

In addition to the statistical analysis of the proposed FEM model results, the ultimate axial strength results predicted using the formulas modified from ACI [39], EC4 [48], and AISC [49], as well as the empirical models suggested by Uenaka et al. [2], Han et al. [50], Yu et al. [51], and Hassanein et al. [52], were also analyzed using the GLM-ANOVA technique. The statistical analysis results for each model are presented in Table 5. According to the statistically evaluation of the results of the modified ACI [39] and AISC [49] formulas and the empirical models suggested by Uenaka et al. [2], Han et al. [50], Yu et al. [51], and Hassanein et al. [52], it is clearly seen that all independent variables have significant effect on the ultimate axial strength determination, yet with different percent contribution values. Nevertheless, the statistical analysis of the results predicted using the modified EC4 [48] formula revealed that the inner steel tube thickness does not have a significant effect on the ultimate axial strength of the CFDST columns because it has the P value of 0.120. Furthermore, the statistical evaluation of the results of all predictive models indicated that the most important independent variable is the outer steel tube diameter since its percent contribution value is more than 65% in the analysis results of all models. The second significant parameter is the concrete compressive strength and the outer steel tube thickness is the third

important independent variable for the ultimate axial strength determination. According to all model results, the lowest effect belongs to the inner steel tube diameter and thickness when the percent contribution values are considered.

7 Conclusions

In this study, it is aimed to model the behavior of axially loaded CFDST composite columns using the FEM. The effects of geometrical and material properties on the load-carrying capacity of the columns are investigated statistically. Even though there are many numerical models modified from the codes and proposed by other researchers to predict the ultimate axial strength of the CFDST columns, the FEM provides additionally the load–deflection curves and deformed shapes of such composite columns. These could be considered as the most remarkable advantages of FEM. Besides, there are other benefits of using the FEM model in proposing the predictive models for the capacity of CFDST columns. Individual definitions of material behavior and properties as well as easily incorporating the boundary conditions could be taken into account other significant gains of the FEM model. On the other hand, the requirement of a large amount of data for the material definition and mesh description could be regarded as the main disadvantage of the FEM model. The following conclusions could be drawn based on the findings above:

- The FEM could be a useful tool for the modeling of the CFDST columns with CHS. The model proposed by FEM has the veridical ultimate axial strengths, which means no zero values or no under zero values. The most significant side of this work is that the FEM model proposed in this study has been verified by various results from the researches available in the literature. This means that the model could be efficiently employed in

predicting the ultimate axial strength of CFDST composite columns.

- The experimental test results of the samples, which were used to verify the FEM model, indicated that the proposed FEM model has good prediction capableness in the estimation of ultimate axial strength and axial stiffness. The FEM model has the average normalized ultimate axial strength value of 1.037 and a coefficient of variation value of 0.093. Besides, the mean absolute percent error value is 7.22.

- The verified FEM model indicated that the ultimate axial strengths of the CFDST columns were affected by the outer and inner steel tubes diameters and thicknesses and the concrete compressive strength. According to the FEM model, when the outer steel tube diameter and thickness increased, the ultimate axial strength also raised. As well, the FEM model results showed that increasing the concrete compressive strength increased the load-carrying capacity of the CFDST columns.

- The CFDST column specimens used in the prediction by the FEM model were also handled in the prediction by the modified code formulas and the proposed empirical models by the researchers. The results revealed that the near prediction performance belongs to the modified EC4 formula. Generally, the modified EC4 formula and the empirical model suggested by Uenaka et al. have the overestimated results; while the others have the underestimated results.

- The predicted results were also statistically analyzed by means of the general linear model analysis of variance technique. The analysis of the FEM model results indicated that all independent parameters have a significant effect on the ultimate axial strength of the CFDST columns according to P values, but the highest effectiveness degree belongs to the outer steel tube diameter regarding the percent contribution. Also, it is noticed that the effectiveness level of the inner steel tube diameter and thickness can be disregarded.

- Besides, the statistical analysis of other models shows similar results with the proposed FEM model except for the statistical analysis of the modified EC4 formula results. According to evaluating the results of the modified EC4 formula statistically, it is noticed that the thickness of the inner steel tube has a P value of 0.120 and it means that the inner steel tube has no significant effect on the ultimate axial strength determination.

Compliance with ethical standards

Conflict of interest The authors declare that there is no conflict of interest regarding the publication of this paper.

Ethical statement Authors state that the research was conducted according to ethical standards.

References

1. Spannverbund. Composite columns. http://www.spannverbund.de/index.php/en/composite-columns.html. Accessed 18 Apr 2019.
2. Uenaka K, Kitoh H, Sonoda K. Concrete filled double skin circular stub columns under compression. Thin Wall Struct. 2010;48:19–24.
3. Zhao XL, Han LH. Double skin composite construction. Prog Struct Mat Eng. 2006;8:93–102.
4. Kalemi B. Numerical modeling and assessment of circular concrete-filled steel tubular members. Master in Science Thesis. Istituto Universitario di Studi Superiori di Pavia; 2016.
5. Hsiao PC, Hayashi KK, Nishi R, Lin XC, Nakashima M. Investigation of concrete-filled double-skin steel tubular columns with ultrahigh-strength steel. J Struct Eng. 2015;141(7):04014166.
6. Furlong RW. Strength of steel-encased-concrete beam columns. J Struct Div. 1967;93:113–24.
7. Chen WF, Chen CH. Analysis of concrete filled steel tubular beam-columns. Int Assoc Bridg Struct Eng Publ. 1973;33(11):37–52.
8. Lin CY. Axial capacity of concrete infilled cold-formed steel columns. In: Proceeding of ninth international specialty conference on cold-formed steel structures. St. Louis, Missouri, USA; 1988.
9. Luksha LK, Nesterovich AP. Strength testing on larger-diameter concrete filled steel tubular members. In: Proceeding 3rd international conference on steel-concrete composite structures; 1991.
10. Prion HGL, Boehme J. Beam-column behavior of steel tubes filled with high strength concrete. Can J Civ Eng. 1994;21(2):207–18.
11. Kato B. Compressive strength and deformation capacity of concrete-filled tubular stub columns. Part I: strength and rotation capacity of concrete-filled tubular columns. J Struct Construct Eng. 1995;468:183–91.
12. Morino S, Sakino K, Mukai A, Yoshioka K. Experimental studies of CFT column systems: US-Japan cooperative earthquake research. New York: ASCE; 1997. p. 1106–10.
13. O'Shea MD, Bridge RQ. Design of circular thin-walled concrete filled steel tubes. J Struct Eng. 2000;11:1295–303.
14. Elchalakani M, Zhao XL, Grzebieta RH. Concrete filled circular steel tubes subjected to pure bending. J Constr Steel Res. 2001;57(11):1141–68.
15. Elremaily A, Azizinamini A. Behavior and strength of circular concrete-filled tube columns. J Constr Steel Res. 2002;58(12):1567–91.
16. Han LH, Yang YF, Tao Z. Concrete-filled thin-walled steel SHS and RHS beam-columns subjected to cyclic loading. Thin Wall Struct. 2003;41(9):801–33.
17. Fujimoto T, Mukai A, Nishiyama I, Sakino K. Behavior of eccentrically-loaded concrete-filled steel tubular columns. J Struct Eng. 2004;2:203–12.
18. Wheeler A, Bridge R. The behavior of circular concrete-filled thin-walled steel tubes in flexure. In: Composite construction in steel and concrete V proceeding 5th engineering international conference, ASCE, Reston, VA; 2006. pp. 412–23.
19. Goode CD, Lam D. Concrete-filled tube columns: tests compared with Eurocode 4. In: Composite construction in steel and concrete

VI proceeding engineering international conference, ASCE, Reston, VA; 2008. pp. 317–25.

20. Zhang GW, Xiao Y, Kunnath S. Low-cycle fatigue damage of circular concrete-filled tube columns. ACI Struct J. 2009;106(2):151–9.

21. Roeder CW, Lehman DE, Bishop E. Strength and stiffness of circular concrete-filled tubes. J Struct Eng. 2010;136:1545–53.

22. Ho JCM, Lai MH. Behaviour of uni-axially loaded CFST columns connected by tie bars. J Constr Steel Res. 2013;83:37–50.

23. Lu ZH, Zhao YG. Suggested empirical models for the axial capacity of circular CFT stub column. J Constr Steel Res. 2010;66:850–62.

24. Nour AI, Güneyisi EM. Prediction model on compressive strength of recycled aggregate concrete filled steel tube columns. Compos B. 2019;173:106938.

25. Güneyisi EM, Gültekin A, Mermerdaş K. Ultimate capacity prediction of axially loaded CFST short columns. Int J Steel Struct. 2016;16(1):99–104.

26. Essopjee Y, Dundu M. Performance of concrete-filled double-skin circular tubes in compression. Compos Struct. 2015;133:1276–83.

27. Zhao XL, Grzebieta RH, Elchalakani M. Tests of concrete-filled double skin CHS composite stub columns. Steel Compos Struct. 2002;2(2):129–42.

28. Tao Z, Han LH, Zhao XL. Behaviour of concrete-filled double skin (CHS outer and CHS inner) steel tubular stub columns and beam-columns. J Constr Steel Res. 2004;60(8):1129–58.

29. Han LH, Li YJ, Liao FY. Concrete-filled double skin steel tubular (CFDST) columns subjected to long-term sustained loading. Thin Wall Struct. 2011;49:1534–43.

30. Wang J, Liu W, Zhou D, Zhu L, Fang H. Mechanical behaviour of concrete filled double skin steel tubular stub columns confined by FRP under axial compression. Steel Compos Struct. 2014;14(4):431–52.

31. Lu H, Zhao XL, Han LH. Testing of self-consolidating concrete-filled double skin tubular stub columns exposed to fire. J Constr Steel Res. 2010;66:1069–80.

32. Wang F, Young B, Gardner L. Experimental investigation of concrete-filled double skin tubular stub columns with stainless steel outer tubes. In: Eighth international conference on steel and aluminium structures Hong Kong, China; 2016.

33. Hu HT, Su FC. Nonlinear analysis of short concrete-filled double skin tube columns subjected to axial compressive forces. Mar Struct. 2011;24:319–37.

34. Pagoulatou M, Sheehan T, Dai XH, Lam D. Finite element analysis on the capacity of circular concrete-filled double-skin steel tubular (CFDST) stub columns. Eng Struct. 2014;72:102–12.

35. Hassanein MF, Kharoob OF. Analysis of circular concrete-filled double skin tubular slender columns with external stainless steel tubes. Thin Wall Struct. 2014;79:23–37.

36. Abaqus. Analysis user's manuals and example problems manuals, version 614. Providence: Dassault Systemes Simulia Corp.; 2014.

37. Han LH, Huo JS. Concrete-filled HSS columns after exposure to ISO-834 standard fire. J Struct Eng. 2003;129(1):68–78.

38. Hu HT, Huang CH, Wu MH, Wu YM. Nonlinear analysis of axially loaded concrete-filled tube columns with confinement effect. J Struct Eng. 2003;129(10):1322–9.

39. ACI-318. Building code requirements for reinforced concrete. American Concrete Institute; 2002.

40. Mander JB, Priestly MJN, Park R. Theoretical stress-strain model for confined concrete. J Struct Eng. 1988;114(8):1804–26.

41. Rirchart FE, Brandzaeg A, Brown RL. A study of the failure of concrete under combined compressive stresses Bull, vol. 185. Champaign: University of Illinois Engineering Experimental Station; 1928.

42. Saenz LP. Discussion of 'Equation for the stress-strain curve of concrete' by P. Desayi, and S. Krishman. J Am Concrete Inst. 1964;61:1229–35.

43. Hu HT, Schnobrich WC. Constitutive modeling of concrete by using nonassociated plasticity. J Mater Civ Eng. 1989;1(4):199–216.

44. Ellobody E, Young B. Nonlinear analysis of concrete-filled steel SHS and RHS columns. Thin Wall Struct. 2006;44:919–30.

45. Ellobody E, Young B. Design and behavior of concrete-filled cold-formed stainless steel tube columns. Eng Struct. 2006;28:716–28.

46. Giakounnelis G, Lam D. Axial capacity of circular concrete-filled tube columns. J Constr Steel Res. 2004;60(7):1049–68.

47. Damaraju AV. Investigation on the stability of noncompact and slender concrete filled tubes subjected to axial loads. MSc Thesis, University of Cincinnati, India; 2013.

48. Eurocode 4. Design of composite steel and concrete structures—Part 1.1: general rules and rules for buildings. London: British Standard Institution, ENV 1994-1-1; 2004.

49. AISC. Load and resistance factor design specification, for structural steel buildings. Chicago: American Institute of Steel Construction; 2010.

50. Han LH, Ren QX, Li W. Tests on stub stainless steel-concrete-carbon steel double-skin tubular (DST) columns. J Constr Steel Res. 2011;67:437–52.

51. Yu M, Zha X, Ye J, Li Y. A unified formulation for circle and polygon concrete-filled steel tube columns under axial compression. Eng Struct. 2013;49:1–10.

52. Hassanein MF, Kharoob OF, Liang QQ. Circular concrete-filled double skin tubular short columns with external stainless steel tubes under axial compression. Thin Wall Struct. 2013;73:252–63.

53. Eurocode 3. Design of steel structure—Part 1.1: general rules and rules for buildings. London: British Standard Institution, ENV 1993-1-1; 2004.

54. AIJ. Standard for structural calculation of steel reinforced concrete structures; 2002 **(in Japanese)**.

55. Hassanein MF, Kharoob OF. Compressive strength of circular concrete-filled double skin tubular shorts columns. Thin Wall Struct. 2014;77:165–73.

56. Liang QQ, Fragomeni S. Nonlinear analysis of circular concrete-filled steel tubular short columns under axial loading. J Constr Steel Res. 2009;65(12):2186–96.

57. Hassanein MF, Kharoob OF, Liang QQ. Behaviour of circular concrete-filled lean duplex stainless steel tubular short columns. Thin Wall Struct. 2013;68:113–23.

58. Liang QQ. Performance-based analysis of concrete-filled steal tubular beam-columns. Part I: theory and algorithms. J Constr Steel Res. 2009;65(2):363–73.

59. Tang J, Hino S, Kuroda I, Ohta T. Modeling of stress-strain relationships for steel and concrete in concrete filled circular steel tubular columns. Steel Constr Eng JSSC. 1996;3(11):35–46.

60. Zhao XL, Tong LW, Wang XY. CFDST stub columns subjected to large deformation axial loading. Eng Struct. 2010;32(3):692–703.

61. Lin ML, Tsai KC. Mechanical behavior of double-skinned composite steel tubular columns. In: Proceedings of the joint NCREE-JRC conference, Taipei, Taiwan; 2003.

62. Dong CX, Ho JCM. Improving interface bonding of double-skinned CFST columns. Mag Concrete Res. 2013;65(20):1199–211.

63. Minitab R12. Statistical tool. Quality Plaza, 1829 Pine Hall Rd., State College, PA, 16801-3008, USA.